SIAM J. Applied Dynamical Systems
Vol. 17, No. 1, pp. 982–1022

Anomalous Scaling of Hopf Bifurcation Thresholds for the Stability of Localized Spot Patterns for Reaction-Diffusion Systems in Two Dimensions*

J. C. Tzou†, M. J. Ward†, and J. C. Wei†

Abstract. For three specific singularly perturbed two-component reaction diffusion systems in a bounded two-dimensional domain admitting localized multispot patterns, we provide a detailed analysis of the parameter values for the onset of temporal oscillations of the spot amplitudes. The two key bifurcation parameters in each of the RD systems are the reaction-time parameter τ and the inhibitor diffusivity D. In the limit of large diffusivity $D = D_0/\nu \gg 1$ with $D_0 = \mathcal{O}(1)$, $\nu \equiv -1/\log\varepsilon$, and ε^2 denoting the activator diffusivity, a leading-order-in-ν analysis shows that the linear stability of multispot patterns is determined by the spectrum of a class of nonlocal eigenvalue problems (NLEPs). The specific form for these NLEPs depends on whether $\tau = \mathcal{O}(1)$ or $\tau \gg 1$. For $D_0 < D_{0c}$, where $D_{0c} > 0$ is some critical threshold, we show from a new parameterization of the NLEP that no Hopf bifurcations leading to temporal oscillations in the spot amplitudes can occur for any $\mathcal{O}(1)$ value of the reaction-time parameter τ. This resolves a long-standing open problem in NLEP theory (see [J. Wei and M. Winter, *Mathematical aspects of pattern formation in biological systems*, Appl. Math. Sci. 189, Springer, 2014]). Instead, by deriving a new modified NLEP appropriate to the regime $\tau \gg 1$, we show for the range $D_0 < D_{0c}$ that a Hopf bifurcation will occur at some $\tau = \tau_H \gg 1$, where τ_H has the anomalous scaling law $\tau_H \sim \nu^{-1}\varepsilon^{-\tau_c} \gg 1$ for some τ_c satisfying $0 < \tau_c < 2$. The anomalous exponent τ_c is calculated from the modified NLEP for each of the three RD systems.

Key words. spot patterns, Hopf bifurcation, nonlocal eigenvalue problem, anomalous scaling, Green's matrix

AMS subject classifications. 35K57, 35P05, 35B25

DOI. 10.1137/17M1137759

1. Introduction.

In the large diffusivity ratio limit, two-component reaction-diffusion (RD) systems can exhibit a surprisingly wide variety of two-dimensional (2-D) spatially localized structures including spot, stripe, and labyrinthian patterns, depending on the specific form of the nonlinear reaction kinetics (cf. [21], [15], [16]). Localized spot patterns are those for which one of the two solution components is highly localized at certain discrete points in the 2-D domain. In the absence of any $\mathcal{O}(1)$ time-scale instability of the spot profile, the spatial locations of the spots will typically evolve slowly toward some steady-state spot configuration. For a few specific RD systems in the singularly perturbed limit of a large diffusivity ratio, localized spot patterns have been shown to exhibit various types of instabilities and dynamical behaviors such as spot self-replication, temporal oscillations in the spot amplitudes, spot annihilation due to overcrowding, and slow spot drift (cf. [27], [10], [28], [29]. [30], [31], [11], [3], [17], [9], [18], [19], [23]).

*Received by the editors July 7, 2017; accepted for publication (in revised form) by Y. Nishiura November 16, 2017; published electronically March 29, 2018.
http://www.siam.org/journals/siads/17-1/M113775.html
Funding: The work of the second and third authors was supported by NSERC Discovery grants. The work of the first author was partially supported by a PIMS CRG Postdoctoral Fellowship.
†Department of Mathematics, University of British Columbia, Vancouver, BC, Canada (tzou.justin@gmail.com, ward@math.ubc.ca, jcwei@math.ubc.ca).

In this paper we provide a detailed study of the onset of temporal oscillations in the spot amplitudes for three prototypical singularly perturbed two-component RD systems in bounded 2-D domains, resolving a key open problem arising in the original linear stability analyses of [27], [28], [29], [30], [31]. In the simpler 1-D setting, the conditions for the onset of oscillations for localized spike solutions due to a Hopf bifurcation have been established for many RD models. (See [5], [6], [25], [12], [2], [4], [20] and some of the references therein.) More recently, [22] has developed a weakly nonlinear theory to unfold the Hopf bifurcation and determine whether 1-D spike amplitude oscillations are subcritical or supercritical. In contrast to this now well-studied 1-D problem, the corresponding problem for 2-D spot amplitude oscillations is less well understood. By using a theoretical framework based on a nonlocal eigenvalue problem (NLEP) we will discuss and then address a key open question regarding the onset of spot amplitude oscillations for multispot patterns in 2-D domains.

Our analysis will be applied to three prototypical systems posed in a bounded 2-D domain Ω. The first model is the standard Gierer–Meinhardt (GM) system (see [27])

$$v_t = \varepsilon^2 \Delta v - v + v^2/u\,, \qquad \tau u_t = D\Delta u - u + \varepsilon^{-2} v^2\,, \qquad \mathbf{x} \in \Omega\,. \tag{1.1}$$

The second system is the nondimensional Gray–Scott (GS) model, given in the scaling regime of [30] by

$$v_t = \varepsilon^2 \Delta v - v + \mathcal{A} u v^2\,, \qquad \tau u_t = D\Delta u + 1 - u - \varepsilon^{-2} u v^2\,, \qquad \mathbf{x} \in \Omega\,. \tag{1.2}$$

Lastly, in the scaling regime of [31], our third system is the nondimensional Schnakenberg model given by

$$v_t = \varepsilon^2 \Delta v - v + \mathcal{A} u v^2\,, \qquad \tau u_t = D\Delta u + 1 - \varepsilon^{-2} u v^2\,, \qquad \mathbf{x} \in \Omega\,. \tag{1.3}$$

In each of these RD systems we impose the no-flux conditions $\partial_n v = 0$ and $\partial_n u = 0$ on $\partial\Omega$. In (1.2) and (1.3) we refer to $\mathcal{A} = \mathcal{O}(1)$ as the feed-rate parameter.

In the limit $\varepsilon \to 0$, each of these three RD systems admits localized N-spot quasi-equilibrium solutions where v concentrates on a set of discrete points $\mathbf{x}_1, \ldots, \mathbf{x}_N$ in Ω. For these solutions, we will analyze the onset of spot amplitude temporal oscillations due to a Hopf bifurcation as the reaction-time parameter τ exceeds a critical value. Our analysis will focus on the regime, considered originally in [26], [27], [28], [29], [30], [31], where $D = \mathcal{O}(\nu^{-1}) \gg 1$ with $\nu \equiv -1/\log\varepsilon$. It is on this range of D where, to leading order in ν and for $\tau = \mathcal{O}(1)$, the linear stability properties of a quasi-equilibrium N-spot pattern are characterized by the spectrum of a radially symmetric NLEP of the form

$$L_0\Psi - \chi(\tau\lambda) w^2 \frac{\int_0^\infty w\Psi\rho\,d\rho}{\int_0^\infty w^2\rho\,d\rho} = \lambda\Psi\,; \qquad \Psi'(0) = 0\,, \quad \Psi \to 0 \quad \text{as} \quad \rho \to \infty\,, \tag{1.4a}$$

where $\chi(z)$ is called the *multiplier* of the nonlocal term. Here $\Psi = \Psi(\rho)$ and the local operator L_0 is defined by

$$L_0\Psi \equiv \Delta_\rho \Psi - \Psi + 2w\Psi\,, \tag{1.4b}$$

where $\Delta_\rho \equiv \partial_{\rho\rho} + \rho^{-1}\partial_\rho$. In this NLEP, $w(\rho)$ is the unique radially symmetric ground-state solution satisfying

$$\Delta_\rho w - w + w^2 = 0\,, \quad 0 < \rho < \infty\,; \quad w(0) > 0\,, \quad w'(0) = 0\,; \quad w \to 0 \quad \text{as} \quad \rho \to \infty\,. \tag{1.4c}$$

The eigenvalues λ of the NLEP (1.4) in $\mathrm{Re}(\lambda) > 0$ correspond to instabilities in the amplitudes of the spots in the sense that, for some function $\Phi_j(\rho)$ related to $\Psi(\rho)$ by an orthogonal matrix $\mathcal{Q}$ involving the eigenvectors of an eigenvalue-dependent Green's matrix (see (A.22) of Appendix A), the perturbation to the quasi-equilibrium solution v_e has the form

$$v = v_e + \sum_{j=1}^{N} c_j \Phi_j \left[\varepsilon^{-1}|\mathbf{x} - \mathbf{x}_j|\right] e^{\lambda t}\,. \tag{1.5}$$

For each of these three RD systems, in the asymptotic regime where $\tau = \mathcal{O}(1)$ and $D = D_0/\nu \gg 1$ with $D_0 = \mathcal{O}(1)$, there are exactly two possible choices for the multiplier $\chi(z)$ corresponding to either synchronous or asynchronous perturbations in the spot amplitudes characterized by either $(c_1, \dots c_N) = (1, \dots, 1)^T$ or $\sum_{j=1}^N c_j = 0$, respectively (cf. [27], [28], [29], [30], [31]). For the $N-1$ distinct *asynchronous modes*, an analysis of the resulting NLEP for each of these three RD systems [27], [28], [29], [30], [31] has proved that there is a model-specific critical value D_{0c} of D_0 for which the multispot pattern is linearly stable to asynchronous perturbations iff $D_0 < D_{0c}$. For $D_0 > D_{0c}$, this linear instability of the spot amplitudes is referred to as a competition instability since, owing to $\sum_{j=1}^N c_j = 0$, it preserves the average spot amplitude. From full numerical computations of the RD systems this linear instability mechanism has been found to trigger a nonlinear process through which one or more spots are annihilated in finite time (cf. [3], [17], [19]).

For the *synchronous mode*, where $c_j = 1$ for $j = 1, \dots, N$, for each of the three RD systems the multiplier $\chi(z)$ of the NLEP is a bilinear function when $D = D_0/\nu$ and $\tau = \mathcal{O}(1)$. From an analysis of the NLEP (1.4) with this bilinear multiplier, the synchronous mode is known to undergo a Hopf bifurcation at some value $\tau = \tau_H$ whenever $D_0 > D_{0c}$ (cf. [27], [28], [29], [30], [31]). As a result, on the range $D_0 > D_{0c}$ where the asynchronous modes are unstable for any $\tau > 0$, an additional instability due to a Hopf bifurcation associated with the synchronous mode will occur when τ exceeds some threshold τ_H. This threshold depends on D_0 but is independent of the spatial configuration of spots.

A key long-standing open problem in NLEP theory for 2-D spot patterns has been to determine whether there is a Hopf bifurcation for the synchronous mode on the range $D_0 < D_{0c}$ where the asynchronous modes are linearly stable (cf. [33]). For $D_0 < D_{0c}$, and for each of the three RD systems above, the rigorous NLEP results in [27], [28], [29], [30], [31] for the synchronous mode have established that $\mathrm{Re}(\lambda) < 0$ when either $0 < \tau < \tau_2$ or $\tau > \tau_3$ for some positive constants τ_2 and τ_3. Therefore, no Hopf bifurcations occur for the synchronous mode when τ is either sufficiently small or large. Since it is unknown whether $\tau_3 = \tau_2$ or $\tau_3 > \tau_2$, a central open problem (cf. [33]) in NLEP theory for 2-D spot patterns is to determine whether a Hopf bifurcation can occur for some intermediate range of τ when $D_0 < D_{0c}$.

For each of the three RD systems we will use a combination of analytical and numerical methods, based on the NLEP (1.4), to show that there is no $\mathcal{O}(1)$ Hopf bifurcation threshold

value of τ for the synchronous mode when $D_0 < D_{0c}$. By rederiving and then analyzing a new class of NLEPs appropriate to the regime $D = D_0/\nu \gg 1$, but with $\tau \gg 1$, we will show analytically that when $D_0 < D_{0c}$ there is a Hopf bifurcation threshold τ_H of τ with the *anomalous scaling* $\tau_H \sim \nu^{-1}\varepsilon^{-\tau_c} \gg 1$ for some τ_c satisfying $0 < \tau_c < 2$. The key implication of our main result is that when $D < D_{0c}/\nu$ and for any $\tau = \mathcal{O}(1)$, quasi-equilibrium multispot patterns are linearly stable on $\mathcal{O}(1)$ time-scales and will therefore exhibit slow spot dynamics (cf. [3], [11], [10]) toward a true steady-state configuration.

A detailed outline of this paper is as follows:

In section 2 we develop a new rigorous winding number approach to analyze the NLEP (1.4) when the multiplier $\chi(z)$ is a bilinear function. As discussed above, such a bilinear multiplier is relevant for analyzing the linear stability of multispot patterns for our three RD systems when $D = D_0/\nu \gg 1$ and $\tau = \mathcal{O}(1)$. We derive some new specific conditions in terms of the coefficients in the bilinear multiplier that determine the number of unstable eigenvalues in $\mathrm{Re}(\lambda) > 0$ of the NLEP (1.4). These results are then applied to our three RD systems, but are not sufficiently refined for resolving whether there is a Hopf bifurcation for the synchronous mode when $D_0 < D_{0c}$.

To address this issue for each of our three RD systems, in section 2 we formulate and numerically implement a new parameterization of any Hopf bifurcation threshold τ_H of τ for the NLEP (1.4) with a bilinear multiplier. For $D_0 > D_{0c}$ our parameterization shows that there is a unique Hopf threshold $\tau = \tau_H$ on $D_0 > D_{0c}$ with corresponding Hopf eigenvalue $\lambda = i\lambda_{IH}$ and $\lambda_{IH} > 0$. As $D_0 \to D_{0c}^+$ we will show that $\tau_H \to +\infty$ and $\lambda_{IH} \to 0^+$ and derive a new analytical scaling law for this limiting behavior. Most importantly, however, is that our new parameterization reveals that there is no $\mathcal{O}(1)$ Hopf bifurcation threshold value of τ for the synchronous mode when $D_0 < D_{0c}$. Thus, we conclude from this leading-order-in-ν NLEP theory that N-spot quasi-equilibrium patterns are linearly stable for any $\tau = \mathcal{O}(1)$ whenever $D < D_{0c}/\nu$.

Motivated by our observation that $\tau_H \to +\infty$ as $D_0 \to D_{0c}^+$, in section 3 we analyze a new class of NLEPs, not considered previously in [27], [28], [29], [30], [31], which is relevant to the asymptotic regime $D = \mathcal{O}(\nu^{-1})$, $\tau \gg 1$ with $\tau\lambda/D \gg 1$. The asymptotic derivation of these new modified NLEPs for each of the three models is given in the three appendices. By analyzing these modified NLEPs for each of the three RD systems, in sections 3.1–3.3 we will show that when $D_0 < D_{0c}$ there is a Hopf bifurcation threshold τ_H with the anomalous scaling $\tau_H \sim \nu^{-1}\varepsilon^{-\tau_c}$ for some τ_c in $0 < \tau_c < 2$. An asymptotic expansion for this anomalous exponent τ_c and for the corresponding Hopf eigenvalue will be derived for each of three RD systems. This anomalous exponent is found to be independent of the spatial configuration of spots.

Our asymptotic result for the anomalous Hopf bifurcation threshold is not uniformly valid as $D_0 \to D_{0c}^-$, since our analysis of the anomalous exponent requires that the strict inequality $\tau_c > 0$ must hold. For $D_0 \to D_{0c}^-$, the Hopf threshold τ_H does depend on the spatial configuration of the spots. For the GM (1.1) and Schnakenberg (1.3) systems, in section 4 we numerically compute the Hopf bifurcation threshold from the modified NLEP for the simple spatial configuration of a ring pattern of spots inside the unit disk.

For the Schnakenberg model (1.3), in section 5 we extend the leading-order-in-ν NLEP theory to derive a globally coupled eigenvalue problem (GCEP) that characterizes the linear

stability of multispot patterns, while accounting for all terms in powers of ν. Although the study of this GCEP is intractable analytically, we numerically compute from it the Hopf bifurcation threshold for a ring pattern of spots in the unit disk. The resulting asymptotic prediction of the Hopf threshold for spot amplitude oscillations is then favorably compared with full numerical results computed from the Schnakenberg model (1.3) using FlexPDE6 [7]. Finally, in section 6, we conclude with a brief discussion.

2. A class of NLEPs with a bilinear multiplier. For the parameter range where $D = \mathcal{O}(\nu^{-1})$ with $\nu \equiv -1/\log\varepsilon$ and for $\tau = \mathcal{O}(1)$, the linear stability on an $\mathcal{O}(1)$ time-scale of N-spot quasi-equilibrium solutions for either (1.1), (1.2), or (1.3) can be reduced to the study of an NLEP of the form (1.4a), where the multiplier $\chi(\tau\lambda)$ of the nonlocal term is a bilinear function of λ of the form

$$\chi(\tau\lambda) = \frac{c + d\tau\lambda}{e + f\tau\lambda}\,, \tag{2.1}$$

where c, d, e, and f are real positive constants and $\tau \geq 0$. It is then readily shown that the discrete eigenvalues of (1.4) are the roots λ of $g(\lambda) = 0$, defined by

$$g(\lambda) = \mathcal{C}(\lambda) - \mathcal{F}(\lambda)\,, \tag{2.2}$$

where

$$\mathcal{C}(\lambda) \equiv \frac{1}{\chi(\tau\lambda)} = \frac{e + f\tau\lambda}{c + d\tau\lambda}\,, \qquad \mathcal{F}(\lambda) \equiv \frac{\int_0^\infty w\left[(L_0 - \lambda)^{-1} w^2\right]\rho\, d\rho}{\int_0^\infty w^2\rho\, d\rho}\,. \tag{2.3}$$

To calculate the number M of discrete eigenvalues of (1.4) in $\mathrm{Re}(\lambda) > 0$, we use the argument principle of complex analysis to determine the number of zeroes of $g(\lambda)$ in $\mathrm{Re}(\lambda) > 0$. We determine the winding number of g over the counterclockwise contour composed of the imaginary axis $-iR_c \leq \mathrm{Im}\lambda \leq iR_c$ and the semicircle Γ_{R_c}, given by $|\lambda| = R_c > 0$ for $|\arg|\lambda \leq \pi/2$, and then let $R_c \to +\infty$. Since $c > 0$ and $d > 0$ in (2.3), $\mathcal{C}(\lambda)$ is analytic in $\mathrm{Re}(\lambda) > 0$. In contrast, $\mathcal{F}(\lambda)$ is analytic in $\mathrm{Re}(\lambda) > 0$ except at the simple pole $\lambda = \nu_0 > 0$, where ν_0 is the unique positive eigenvalue of L_0 (see Theorem 2.12 of [14]). For $R_c \to \infty$, we have on Γ_{R_c} that $|\mathcal{C}(\lambda)|$ is bounded and $|\mathcal{F}(\lambda)| = \mathcal{O}\left(1/|\lambda|\right) \ll 1$. As such, there is no change in the argument of g over Γ_{R_c} as $R_c \to \infty$. Then, by using $g(\overline{\lambda}) = \overline{g(\lambda)}$, and assuming that there are no zeros of $g(\lambda)$ on the imaginary axis, we get

$$M = 1 + \frac{1}{\pi}\left[\arg g\right]_{\Gamma_I}\,, \tag{2.4}$$

where $\left[\arg g\right]_{\Gamma_I}$ denotes the change in the argument of g along the semi-infinite imaginary axis $\Gamma_I = i\lambda_I$ with $0 \leq \lambda_I < \infty$, traversed in the downward direction.

To calculate $\left[\arg g\right]_{\Gamma_I}$, where $\lambda = i\lambda_I$ with $0 < \lambda_I < \infty$, we decompose $g(i\lambda_I)$ into real and imaginary parts, as $g(i\lambda_I) = g_R(\lambda_I) + ig_I(\lambda_I)$, to get

$$g_R(\lambda_I) = \mathcal{C}_R(\lambda_I) - \mathcal{F}_R(\lambda_I)\,, \qquad g_I(\lambda_I) = \mathcal{C}_I(\lambda_I) - \mathcal{F}_I(\lambda_I)\,, \tag{2.5}$$

where

$$\mathcal{C}_R(\lambda_I) = \frac{ec + df\tau^2\lambda_I^2}{c^2 + d^2\tau^2\lambda_I^2}, \qquad \mathcal{F}_R(\lambda_I) \equiv \frac{\int_0^\infty \rho w L_0 \left[L_0^2 + \lambda_I^2\right]^{-1} w^2\, d\rho}{\int_0^\infty \rho w^2\, d\rho}, \tag{2.6a}$$

$$\mathcal{C}_I(\lambda_I) = \frac{\tau\lambda_I(fc - de)}{c^2 + d^2\tau^2\lambda_I^2}, \qquad \mathcal{F}_I(\lambda_I) \equiv \lambda_I \frac{\int_0^\infty \rho w \left[L_0^2 + \lambda_I^2\right]^{-1} w^2\, d\rho}{\int_0^\infty \rho w^2\, d\rho}. \tag{2.6b}$$

As established rigorously in [24], $\mathcal{F}_R$ and $\mathcal{F}_I$ have the following qualitative properties:

(2.7a)
$$\mathcal{F}_R(\lambda_I) \sim 1 - \kappa_c\lambda_I^2 + \cdots, \quad \text{as} \quad \lambda_I \to 0^+; \quad \mathcal{F}_R'(\lambda_I) < 0 \quad \text{for} \quad \lambda_I > 0; \quad \mathcal{F}_R(\infty) = 0,$$

(2.7b)
$$\mathcal{F}_I(\lambda_I) \sim \lambda_I/2, \quad \text{as} \quad \lambda_I \to 0^+; \quad \mathcal{F}_I(\lambda_I) > 0 \quad \text{for} \quad \lambda_I > 0; \quad \mathcal{F}_I(\infty) = 0,$$

where $\kappa_c > 0$ is given by

$$\kappa_c \equiv \frac{\int_0^\infty \rho\,(w + \rho w'/2)^2\, d\rho}{\int_0^\infty \rho w^2\, d\rho} \approx 0.436. \tag{2.7c}$$

The numerical value for κ_c was obtained by computing the ground-state $w(\rho)$ in (1.4c) numerically. With these basic properties we now establish a few key results for the discrete spectrum of (1.4).

Lemma 2.1. *Let $\tau > 0$ and suppose that $\mathcal{C}_R(0) = e/c < 1$ and $e/c > \mathcal{C}_R(\infty) = f/d$. Then, $M = 0$, and so any discrete eigenvalue of (1.4) satisfies $Re(\lambda) < 0$. In addition, if $\tau = 0$ and $e/c < 1$, then $Re(\lambda) < 0$.*

Proof. Let $\tau > 0$. We have $g(0) = e/c - 1 < 0$ and $g(i\infty) = f/d > 0$, and since $fc - de < 0$ we have upon using (2.7) and (2.6) that $\mathrm{Im}(g(i\lambda_I)) = g_I(\lambda_I) < 0$ for any $\lambda_I > 0$. This proves that $[\arg g]_{\Gamma_I} = -\pi$. Therefore, $M = 0$ from (2.4), and so $\mathrm{Re}(\lambda) < 0$ for any eigenvalue of (1.4).

If $\tau = 0$, we have $g(0) = e/c - 1 < 0$ and $g(i\infty) = e/c > 0$, and $g_I(\lambda_I) = -\mathcal{F}_I(\lambda_I) < 0$ for all $\lambda_I > 0$. Thus, $[\arg g]_{\Gamma_I} = -\pi$, and $M = 0$ from (2.4). Hence, $\mathrm{Re}(\lambda) < 0$ for any eigenvalue of (1.4). ∎

We now establish a condition for which there is a unique positive real eigenvalue for the NLEP (1.4).

Lemma 2.2. *Suppose that $e/c > 1$. If $\tau = 0$, then $M = 1$. If $\tau > 0$ and $f/d > 1$, then $M = 1$ for all $\tau > 0$.*

Proof. If $e/c > 1$ and $\tau = 0$, then from (2.7) and (2.6), we get $g(0) = e/c - 1 > 0$ and $g(i\infty) = e/c > 0$. Since $g_R'(\lambda_I) > 0$, owing to the fact that $\mathcal{F}_R' < 0$ from (2.7), we conclude that $g_R(\lambda_I) > 0$ for $\lambda_I > 0$. Therefore, $[\arg g]_{\Gamma_I} = 0$ and so from (2.4) we get $M = 1$. If $\tau > 0$, $\mathcal{C}_R(0) = e/c > 1$, and $\mathcal{C}_R(\infty) = f/d > 1$, then since $\mathcal{C}_R(\lambda_I)$ is either monotonically increasing or decreasing, we have $\mathcal{C}_R(\lambda_I) > 1$ for all $\lambda_I \geq 0$. Since $\mathcal{F}_R(0) = 1$ and $\mathcal{F}_R(\lambda_I)$ is monotone decreasing on $\lambda_I > 0$, it follows that $g_R(\lambda_I) > 0$ on $\lambda_I \geq 0$. As a result, $[\arg g]_{\Gamma_I} = 0$, and so from (2.4) we get $M = 1$. ∎

Lemma 2.3. *Let $\tau > 0$ and suppose that $\mathcal{C}_R(0) = e/c < 1$ and $e/c < f/d = \mathcal{C}_R(\infty)$. Then, either $M = 0$ or $M = 2$. If $0 < \tau \ll 1$, then $M = 0$. In contrast, if $\tau \gg 1$, then $M = 2$ when $f/d > 1$ and $M = 0$ when $f/d < 1$.*

Proof. Since, from (2.6), $\mathcal{C}_R(\lambda_I)$ is monotone increasing, while from (2.7), $\mathcal{F}_R(\lambda_I)$ is monotone decreasing, and then $g_R(\lambda_I) = 0$ has a unique root $\lambda_I^\star > 0$. We have $g(0) = e/c - 1 < 0$ and $g(i\infty) = f/d > 0$. If $g_I(\lambda_I^\star) < 0$, then $[\arg g]_{\Gamma_I} = -\pi$, and $M = 0$ from (2.4), while if $g_I(\lambda_I^\star) > 0$, then $[\arg g]_{\Gamma_I} = \pi$, and $M = 2$.

If $0 < \tau \ll 1$, we obtain that $\lambda_I^\star = \mathcal{O}(1)$, but $\mathcal{C}_I(\lambda_I^*) = \mathcal{O}(\tau) \ll 1$ from (2.6). Therefore, from (2.7) we have $g_I(\lambda_I^\star) = -\mathcal{F}_I(\lambda_I^\star) + \mathcal{O}(\tau) < 0$, which yields $M = 0$. Next, suppose that $\tau \gg 1$. If $f/d > 1$, then the unique root $\lambda_I^\star > 0$ to $g_R(\lambda_I) = 0$ satisfies $\lambda_I^\star = \mathcal{O}(\tau^{-1}) \ll 1$. Since $fc - de > 0$, we have $\mathcal{C}_I(\lambda_I^\star) = \mathcal{O}(1) > 0$ and $\mathcal{F}_I(\lambda_I^\star) = \mathcal{O}(\tau^{-1})$ from (2.6) and (2.7). This yields that $g_I(\lambda_I^\star) > 0$, and consequently $M = 2$. Alternatively, if $\tau \gg 1$ and $f/d < 1$, then $\lambda_I^\star = \mathcal{O}(1)$ and $\mathcal{C}_I(\lambda_I^\star) = \mathcal{O}(\tau^{-1}) \ll 1$. This yields that $g_I(\lambda_I^\star) < 0$, so that $M = 0$. ∎

Lemma 2.3 establishes that $\mathrm{Re}(\lambda) < 0$ for $\tau \gg 1$ whenever $c/e > 1$ and $d/f > 1$. The next result establishes a precise bound on τ for which $\mathrm{Re}(\lambda) < 0$ holds in this parameter regime.

Lemma 2.4. *Suppose that $e/c < 1$ and $f/d < 1$. Then, any discrete eigenvalue of (1.4) satisfies $Re(\lambda) < 0$ when $\tau > \tau_B \equiv 2(cf - ed)/[3(d - f)^2]$.*

Proof. From equation (5.62) of [32], we have that if $\lambda_R = \mathrm{Re}(\lambda) \geq 0$, then

$$\left(\frac{\int_0^\infty \rho w^3\, d\rho}{\int_0^\infty \rho w^2\, d\rho}\right) \left|\chi(\tau\lambda) - 1\right|^2 + \mathrm{Re}\left[\bar{\lambda}\left(\chi(\tau\lambda) - 1\right)\right] \leq 0\,. \tag{2.8}$$

Since $\int_0^\infty \rho w^3\, d\rho / \int_0^\infty \rho w^2\, d\rho = 3/2$ (see (B.1) and (B.5) of [24]), and upon defining $z \equiv \tau\lambda$, (2.8) becomes

$$\frac{3}{2}\left|\chi(z) - 1\right|^2 + \frac{1}{\tau}\mathrm{Re}\left[\bar{z}\left(\chi(z) - 1\right)\right] \leq 0\,. \tag{2.9}$$

Then, upon using $\chi(z) - 1 = [(c - e) + (d - f)z]/(e + fz)$, we calculate from (2.9) that if $z_R \geq 0$, then

$$\frac{3}{2}\left|c - e + (d - f)z\right|^2 + \frac{1}{\tau}\mathrm{Re}\left[\bar{z}\left(c - e + (d - f)z\right)(e + f\bar{z})\right] \leq 0\,,$$

$$\frac{3}{2}\left|c - e + (d - f)z\right|^2 + \frac{1}{\tau}\mathrm{Re}\left[f(d - f)\bar{z}|z|^2 + e(d - f)|z|^2 + (c - e)f\bar{z}^2 + e(c - e)\bar{z}\right] \leq 0\,.$$

Therefore, if $z_R \geq 0$, then

$$\frac{3}{2}\left(c - e + (d - f)z_R\right)^2 + \frac{1}{\tau}z_R f(d - f)|z|^2 + \frac{1}{\tau}(c - e)f z_R^2 + \frac{1}{\tau}e(d - f)z_R^2 + \frac{e}{\tau}(c - e)z_R + z_I^2\left[\frac{3}{2}(d - f)^2 - \frac{1}{\tau}(cf - ed)\right] \leq 0\,. \tag{2.10}$$

∎

If $c/e > 1$, $z_R \geq 0$, and $d/f > 1$, then the first term is positive, and all remaining terms in (2.10) except the last one are nonnegative. Hence, we have a contradiction to $z_R \geq 0$ if $3(d - f)^2/2 \geq (cf - ed)/\tau$. Thus, if $\tau > \tau_B \equiv 2(cf - ed)/[3(d - f)^2]$, then $\mathrm{Re}(\lambda) < 0$.

2.1. The Gierer–Meinhardt model. In [27] the linear stability on an $\mathcal{O}(1)$ time-scale of an N-spot quasi-equilibrium pattern for the GM model (1.1) was analyzed in the parameter regime $D = \mathcal{O}(\nu^{-1})$ with $\nu \equiv -1/\log\varepsilon \ll 1$, and where $\tau > 0$ satisfies $\tau = \mathcal{O}(1)$ as $\varepsilon \to 0$. To leading order in ν, it was proved in [27] that the linear stability of an N-spot pattern on an $\mathcal{O}(1)$ time-scale is determined by the spectrum of (1.4) where χ has either of the two possible forms

$$\chi_a \equiv \frac{2}{1+\mu}, \qquad \chi_s = \frac{2}{1+\mu}\left(\frac{1+\mu+\tau\lambda}{1+\tau\lambda}\right), \qquad \text{where} \qquad \mu \equiv \frac{2\pi N D_0}{|\Omega|}. \tag{2.11}$$

Here $D_0 \equiv D\nu$ and $|\Omega|$ is the area of Ω. The multipliers χ_a and χ_s correspond to either asynchronous or synchronous perturbations of the spot amplitudes, respectively (see [27]).

For the *asynchronous mode*, with multiplier χ_a, we identify from (2.1) that $e/c = (1+\mu)/2$ and $\tau = 0$. Since $e/c < 1$ iff $\mu < 1$, we conclude from the second statement of Lemma 2.1 that $\mathrm{Re}(\lambda) < 0$ when $0 < \mu < 1$. Alternatively, when $\mu > 1$, the first statement of Lemma 2.2 proves that there is a unique real unstable eigenvalue in $\mathrm{Re}(\lambda) > 0$. Therefore, $\mu = 1$ is the stability threshold for the asynchronous modes.

Next, consider the *synchronous mode*, with multiplier χ_s given in (2.11). From (2.1) we identify that $e/c = 1/2$ and $f/d = (1+\mu)/2$. Since $e/c < 1$ and $e/c < f/d$ for all $\mu > 0$, we conclude from the first statement of Lemma 2.3 that $\mathrm{Re}(\lambda) < 0$ for $0 < \tau \ll 1$. Since $f/d > 1$ iff $\mu > 1$, we conclude from the second statement of Lemma 2.3 that if $\mu > 1$, there are exactly two discrete eigenvalues of (1.4) in $\mathrm{Re}(\lambda) > 0$ when $\tau \gg 1$. Since the multiplier χ_s in the NLEP depends on the product $\tau\lambda$, eigenvalues cannot enter $\mathrm{Re}(\lambda) > 0$ through the origin $\lambda = 0$ as τ is increased. Therefore, by continuity in τ, there must be a Hopf bifurcation (HB) value of τ and complex conjugate eigenvalue pair $\lambda = \pm i\lambda_{IH}$ with $\lambda_{IH} > 0$, possibly nonunique, for the synchronous mode when $\mu > 1$. Alternatively if $0 < \mu < 1$, for which $f/d < 1$, we conclude from Lemma 2.3 that $\mathrm{Re}(\lambda) < 0$ when $\tau \gg 1$. More precisely, Lemma 2.4 yields the bound that $\mathrm{Re}(\lambda) < 0$ when $\tau > \tau_B = 4\mu/[3(1-\mu)^2]$.

A key open question, unresolved from the analysis above or in [27], is whether there is an HB value of τ for the synchronous mode when $0 < \mu < 1$. Our rigorous results above, and obtained in [27], establish that $\mathrm{Re}(\lambda) < 0$ on $0 < \mu < 1$ whenever τ is either sufficiently small or sufficiently large. The open question of [27] for the synchronous mode is to establish whether or not $\mathrm{Re}(\lambda) < 0$ *for all* $\tau > 0$ when $0 < \mu < 1$.

We examine this open question numerically, by developing a new parameterization of any HB value $\tau = \tau_H(\mu)$, as obtained by setting $g(i\lambda_I) = 0$ in (2.5) with (2.11) for χ_s, which yields

$$\frac{(1+\mu)}{2}\left(\frac{1+i\tau\lambda_I}{1+\mu+i\tau\lambda_I}\right) = \mathcal{F}_R(\lambda_I) + i\mathcal{F}_I(\lambda_I). \tag{2.12}$$

We let $\mu = \mu(\lambda_I)$ and $\tau_H(\lambda_I)$ for $\lambda_I > 0$, and after separating (2.12) into real and imaginary parts, we obtain the parameterization

$$\mu = \frac{\left(4|\mathcal{F}|^2 + 1 - \mathcal{F}_R\right)}{2\mathcal{F}_R - 1}, \qquad \tau_H = \frac{2|\mathcal{F}|^2 - \mathcal{F}_R}{\lambda_I \mathcal{F}_I}, \tag{2.13}$$

where $|\mathcal{F}|^2 = \mathcal{F}_R^2 + \mathcal{F}_I^2$. Here we have labelled $\mathcal{F}_R \equiv \mathcal{F}_R(\lambda_I)$ and $\mathcal{F}_I \equiv \mathcal{F}_I(\lambda_I)$.

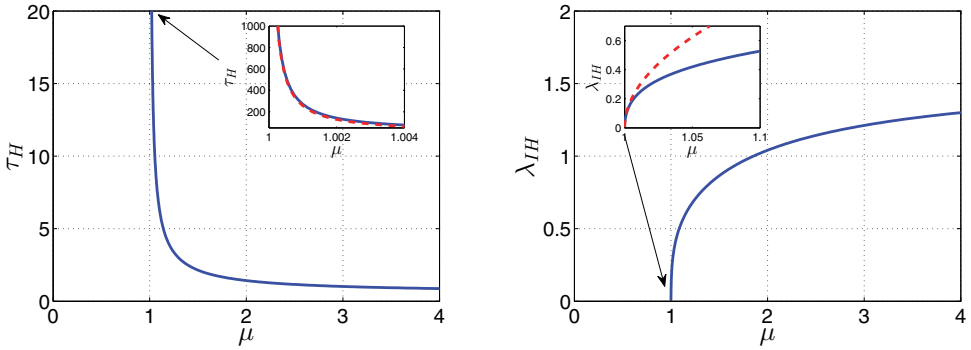

(a) τ_H versus μ (b) λ_{IH} versus μ

Figure 1. *Plot of the HB threshold τ_H (left panel) and imaginary eigenvalue λ_{IH} (right panel) versus μ for the synchronous mode of instability for the GM model, as obtained from (2.13). There is no HB threshold for $\mu < 1$, and $\tau_H \to +\infty$ while $\lambda_{IH} \to 0^+$ as $\mu \to 1^+$. The inserts validate the asymptotic results of (2.14) (dashed curves) for τ_H and λ_{IH} as $\mu \to 1^+$.*

By varying λ_I on $0 < \lambda_I < \infty$, and numerically computing $\mathcal{F}_R$ and $\mathcal{F}_I$ from (2.6), we obtain the Hopf bifurcation curve in the $\mu > 0$ and $\tau > 0$ parameter plane as shown in Figure 1(a). The corresponding eigenvalue, denoted by λ_{IH}, is plotted versus μ in Figure 1(b). From Figure 1(a), (b), we observe that there is a unique HB threshold τ_H for the synchronous mode only on the range $\mu > 1$ and that $\tau_H \to +\infty$ and $\lambda_{IH} \to 0^+$ as $\mu \to 1^+$. Since our computations show that there is no HB threshold value of τ for the range $0 < \mu < 1$, we conclude that the synchronous mode is linearly stable when $\mu < 1$ for any $\tau > 0$, which resolves the open problem of [27]. Since the asynchronous mode is also linearly stable when $0 < \mu < 1$, as we showed above, we conclude that, for any $\tau > 0$ independent of ε, an N-spot quasi-equilibrium pattern is linearly stable on the parameter regime $D = \mathcal{O}(\nu^{-1})$ whenever $D_0 < |\Omega|/(2\pi N)$, where $D = D_0/\nu$.

The asymptotic behavior as $\mu \to 1^+$ and in the shadow-limit $\mu \to \infty$ of the HB threshold in Figure 1 is readily established. For $\mu \to +\infty$, we have that $\lambda_{IH} \to \lambda_{IH\infty}$, where $\lambda_{IH\infty} \approx 1.59$ is the unique root of $\mathcal{F}_R(\lambda_I) = 1/2$. The uniqueness of this root follows from the monotonicity property of $\mathcal{F}_R$ in (2.7). This yields from (2.13) that $\tau_H \to \tau_{H\infty} \equiv 2\mathcal{F}_I(\lambda_{IH\infty})/\lambda_{IH\infty} \approx 0.563$ as $\mu \to \infty$. Now for $\mu \to 1^+$, for which $\lambda_{IH} \to 0$, we use the local behavior as $\lambda_I \to 0$ of $\mathcal{F}_R$ and $\mathcal{F}_I$ given in (2.7b) to readily derive from (2.13) that $\mu \sim 1 + \lambda_I^2(1 - 2\kappa_c) + \cdots$ and $\tau_H \sim 2/\lambda_I^2$. In terms of $\kappa_c \approx 0.436$, as defined in (2.7c), this yields the limiting behavior

$$\tau_H \sim \frac{2(1-2\kappa_c)}{\mu - 1}, \qquad \lambda_{IH} \sim \sqrt{\frac{\mu - 1}{1 - 2\kappa_c}}, \qquad \text{as} \qquad \mu \to 1^+. \tag{2.14}$$

2.2. The Schnakenberg model. In [31] the linear stability of an N-spot quasi-equilibrium pattern for the Schnakenberg model (1.3) was analyzed for the parameter range $D = \mathcal{O}(\nu^{-1})$ with $\nu \equiv -1/\log\varepsilon \ll 1$, where $\tau = \mathcal{O}(1)$ as $\varepsilon \to 0$. To leading order in ν, the analysis in [31] proved that the linear stability of an N-spot pattern on an $\mathcal{O}(1)$ time-scale is determined by the spectrum of (1.4), where there are two choices for the multiplier χ, corresponding to

either asynchronous, χ_a, or synchronous, χ_s, perturbations of the spot amplitudes. These multipliers are given by

$$\chi_a \equiv \frac{2}{1+\alpha}\,, \quad \chi_s = \frac{2\,(\mu+\tau\lambda)}{\mu+(\alpha+1)\tau\lambda}\,, \quad \text{where} \quad \mu \equiv \frac{2\pi N D_0}{|\Omega|}\,, \quad \alpha \equiv \frac{4\pi^2 b D_0 N^2}{|\Omega|^2\mathcal{A}^2}\,. \tag{2.15}$$

Here $D = D_0/\nu$, $|\Omega|$ is the area of Ω, and $b \equiv \int_0^\infty \rho w^2\,d\rho \approx 4.935$, where $w(\rho)$ is the ground-state of (1.4c).

For the *asynchronous mode* with multiplier χ_a, (2.1) yields that $e/c = (1+\alpha)/2$ and $\tau = 0$. From Lemmas 2.1 and 2.2 we conclude that $\mathrm{Re}(\lambda) < 0$ iff $\alpha < 1$ and that there is a unique unstable real eigenvalue of (1.4) when $\alpha > 1$. By using (2.15) for α, we conclude that an N-spot quasi-equilibrium pattern is linearly stable to asynchronous perturbations in the spot amplitudes iff

$$\mathcal{A} > \mathcal{A}_c \equiv \frac{2\pi N}{|\Omega|}\sqrt{bD_0}\,, \qquad b \equiv \int_0^\infty \rho w^2\,d\rho \approx 4.935\,. \tag{2.16}$$

Next, we consider the *synchronous mode* with multiplier χ_s. From (2.15) and (2.1) we identify that $e/c = 1/2$, $f/d = (1+\alpha)/2$, and so $e/c < f/d$ for all $\alpha > 0$. From Lemma 2.3 we conclude that $\mathrm{Re}(\lambda) < 0$ for $0 < \tau \ll 1$. In addition, for $\alpha > 1$ there are exactly two discrete eigenvalues of (1.4) in $\mathrm{Re}(\lambda) > 0$ when $\tau \gg 1$, and so by continuity in τ there must be an HB value of τ, possibly nonunique, for the synchronous mode when $\alpha > 1$. In contrast, when $0 < \alpha < 1$, Lemma 2.3 yields that $\mathrm{Re}(\lambda) < 0$ when $\tau \gg 1$.

This qualitative behavior of an HB threshold for the Schnakenberg model is identical to that for the GM model considered in (2.2). The key open question, unresolved from the analysis above or in [31], is whether there is an HB threshold for τ for the synchronous mode when $0 < \alpha < 1$.

To address this question numerically, we seek a parameterization of any HB value $\tau = \tau_H(\alpha)$ by setting $g(i\lambda_I) = 0$ in (2.5) with (2.15) for χ_s. This involves taking the real and imaginary parts of

$$\frac{(\alpha+1)\tau\lambda_I + \mu}{2\mu + 2i\tau\lambda_I} = \mathcal{F}_R(\lambda_I) + i\mathcal{F}_I(\lambda_I)\,. \tag{2.17}$$

With this characterization, and analogous to (2.13), we readily obtain the following parametric description of the HB threshold in the form $\alpha = \alpha(\lambda_I)$ and $\tau_H(\lambda_I)$ for $\lambda_I > 0$:

$$\alpha = \frac{\left(4|\mathcal{F}|^2 + 1 - \mathcal{F}_R\right)}{2\mathcal{F}_R - 1}\,, \qquad \tau_H = \frac{\mu\,(2\mathcal{F}_R - 1)}{2\lambda_I \mathcal{F}_I}\,. \tag{2.18}$$

By using the local behavior for $\mathcal{F}_R$ and $\mathcal{F}_I$ as $\lambda_I \to 0$ given in (2.7b), we calculate from (2.18) that

$$\tau_H \sim \frac{\mu(1-2\kappa_c)}{\alpha - 1}\,, \qquad \lambda_{IH} \sim \sqrt{\frac{\alpha-1}{1-2\kappa_c}}\,, \qquad \text{as} \qquad \alpha \to 1^+\,. \tag{2.19}$$

By using the parameterization (2.18), in Figure 2 we plot the HB threshold τ_H and corresponding eigenvalue λ_{IH} versus α for a fixed value $\mu = 2$. These results show that there is a

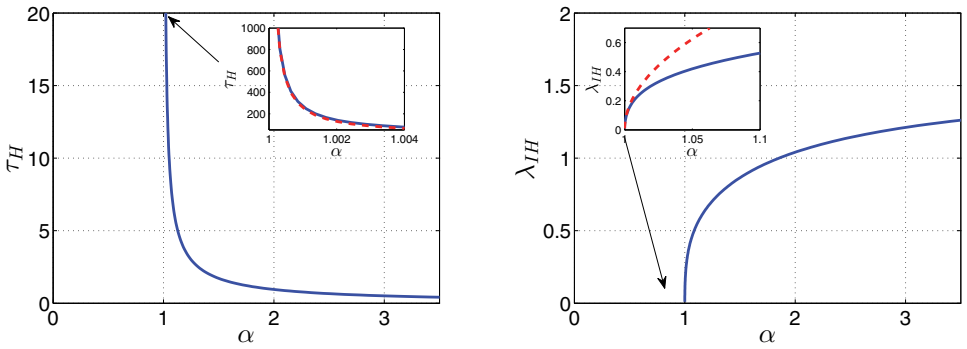

(a) τ_H versus α (b) λ_{IH} versus α

Figure 2. *Plot of the HB threshold τ_H (left panel) and imaginary eigenvalue λ_{IH} (right panel) versus α for the synchronous mode of instability for the Schnakenberg model when $\mu = 2$, as obtained from (2.18). There is no HB threshold for $\alpha < 1$, and $\tau_H \to +\infty$ while $\lambda_{IH} \to 0^+$ as $\alpha \to 1^+$. The asymptotic results given in (2.19) (dashed curves) for τ_H and λ_{IH} as $\alpha \to 1^+$ shown in the two inserts agree well with the numerical results from (2.18).*

unique HB threshold for the synchronous mode only on the range $\alpha > 1$ and that the limiting asymptotic behavior in (2.19) as $\alpha \to 1^+$ agrees well with the numerical results from (2.18). There is no HB threshold value of τ for the range $0 < \alpha < 1$ for the synchronous mode, and so we conclude for this mode that $\mathrm{Re}(\lambda) < 0$ when $0 < \alpha < 1$ for any $\tau > 0$. Owing to the fact that the asynchronous mode is also linearly stable when $0 < \mu < 1$, we conclude that, for any $\tau > 0$ with $\tau = \mathcal{O}(1)$, an N spot quasi-equilibrium pattern is linearly stable on an $\mathcal{O}(1)$ time-scale on the parameter regime $D = \mathcal{O}(\nu^{-1})$ when $\mathcal{A} > \mathcal{A}_c$, where $\mathcal{A}_c$ is defined in (2.16).

2.3. The Gray–Scott model. In [30] the linear stability of an N-spot quasi-equilibrium pattern for the GS model (1.2) was analyzed for the parameter range $D = \mathcal{O}(\nu^{-1})$ and $\mathcal{A} = \mathcal{O}(1)$ with $\nu \equiv -1/\log\varepsilon \ll 1$, where $\tau = \mathcal{O}(1)$ as $\varepsilon \to 0$. A key feature of the GS model in this regime is that quasi-equilibrium multispot patterns exhibit a saddle-node bifurcation structure in which the feed-parameter $\mathcal{A}$ is related to the common spot amplitude, characterized by the parameter S_0, through the nonlinear algebraic equation (see Appendix B)

$$\mathcal{A}_0\mu^{1/2} = (1+\mu)S_0 + \frac{b}{S_0}\,, \qquad \mu \equiv \frac{2\pi N D_0}{|\Omega|}\,, \qquad \mathcal{A}_0 \equiv \mathcal{A}\sqrt{\frac{|\Omega|}{2\pi N}}\,. \tag{2.20}$$

Here $D = D_0/\nu$ and $b \equiv \int_0^\infty \rho w^2\,d\rho \approx 4.935$, where $w(\rho)$ is the ground-state satisfying (1.4c). For $\mu = 2$, the bifurcation diagram of S_0 versus $\mathcal{A}_0$ is shown in Figure 3. The saddle-node bifurcation point where $d\mathcal{A}_0/dS_0 = 0$ occurs at $\mathcal{A}_0 = \mathcal{A}_{0f} \equiv 2\,[b(1+\mu)/\mu]^{1/2}$ when $S_0 = S_{0f} \equiv [b/(1+\mu)]^{1/2}$.

At each point on the bifurcation curve (2.20), the linear stability of the N-spot quasi-equilibrium pattern on an $\mathcal{O}(1)$ time-scale is characterized by the spectrum of the NLEP (1.4), where the multiplier χ has, once again, two distinct forms corresponding to either

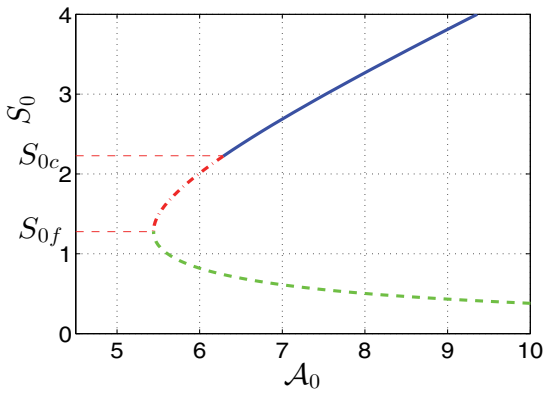

Figure 3. *The bifurcation diagram of the common spot amplitude, measured by S_0, versus the feed-rate parameter $\mathcal{A}_0$ from (2.20) for the GS model with $\mu = 2$. The saddle-node point is at $S_0 = S_{0f} = [b/(1+\mu)]^{1/2}$ and $\mathcal{A}_0 = \mathcal{A}_{0f} \equiv 2\,[b(1+\mu)/\mu]^{1/2}$, where $b \approx 4.935$. On the upper (solid) branch, where $S_0 > S_{0c} \equiv \sqrt{b}$, the asynchronous mode is linearly stable, and the synchronous is linearly stable for all $\tau > 0$. On the middle (dashed) portion, where $S_{0f} < S_0 < S_{0c}$, the asynchronous mode is unstable, and the synchronous mode undergoes a Hopf bifurcation at some $\tau = \tau_H(S_0) > 0$. On the lower (dashed-dotted) branch, where $S_0 < S_{0f}$, the asynchronous mode is unstable, and the synchronous mode is unstable for any $\tau \geq 0$.*

asynchronous or synchronous perturbations of the spot amplitudes (see Appendix B). These multipliers are

$$\chi_a \equiv \frac{2S_0^2}{b+S_0^2}\,, \qquad \chi_s = \frac{2S_0^2\,(1+\mu+\tau\lambda)}{b(1+\tau\lambda)+S_0^2(1+\mu+\tau\lambda)}\,. \tag{2.21}$$

For the *asynchronous mode* with multiplier χ_a, we compare (2.21) and (2.1) to identify that $e/c = (b+S_0^2)/[2S_0^2]$ and $\tau = 0$. We calculate $e/c > 1$ iff $S_0 < S_{0c} \equiv \sqrt{b}$. From Lemma 2.1 and the first statement of Lemma 2.2 we conclude that $\mathrm{Re}(\lambda) < 0$ when $S_0 > S_{0c}$ and that there is a unique unstable real eigenvalue of (1.4) whenever $S_0 < S_{0c}$. As shown in Figure 3 it is only along the solid-shaded portion of the bifurcation curve that the N-spot pattern is linearly stable to asynchronous perturbations. We refer to $S_{0c} \equiv \sqrt{b}$, and the corresponding feed-rate value $\mathcal{A}_0 = \mathcal{A}_{0c} \equiv (2+\mu)\sqrt{b/\mu}$, as the competition-stability threshold.

For the *synchronous mode* with multiplier χ_s, we compare (2.21) and (2.1) to identify e/c and f/d as

$$\frac{e}{c} = \frac{1}{2} + \frac{b}{2S_0^2(1+\mu)}\,, \qquad \frac{f}{d} = \frac{1}{2} + \frac{b}{2S_0^2}\,. \tag{2.22}$$

Since $\mu > 0$, it follows that $e/c < f/d$. We observe that $e/c < 1$ iff $S_0 > S_{0f}$, whereas $f/d < 1$ iff $S_0 > S_{0c}$. On the lower branch (dashed-curve) of the bifurcation curve in Figure 3 where $S_0 < S_{0f}$ we have $1 < e/c < f/d$. From the second statement of Lemma 2.2 we conclude that the NLEP (1.4) has a unique positive real eigenvalue for any $\tau \geq 0$. Therefore, this lower solution branch is unconditionally unstable to synchronous perturbations of the spot amplitudes. Next, along the middle branch (dashed-dotted curve) of the bifurcation curve of Figure 3 where $S_{0f} < S_0 < S_{0c}$, we have $e/c < 1$ while $f/d > 1$. We conclude from Lemma

2.3 that $\mathrm{Re}(\lambda) < 0$ when $\tau \ll 1$ and that there are exactly two discrete eigenvalues of (1.4) in $\mathrm{Re}(\lambda) > 0$ when $\tau \gg 1$. Therefore, along this middle branch, where $S_{0f} < S_0 < S_{0c}$, there must be an HB value of τ, possibly nonunique, for the synchronous mode. A parameterization for this Hopf bifurcation curve is given below in (2.24). Finally, along the upper branch (solid curve) of the bifurcation curve of Figure 3 where $S_0 > S_{0c}$, in which the asynchronous mode is linearly stable, we have $e/c < f/d < 1$. We conclude from Lemma 2.3 that $\mathrm{Re}(\lambda) < 0$ when $0 < \tau \ll 1$ and when $\tau \gg 1$ with no stability information for intermediate values of τ.

The primary open question, unresolved in this analysis and that in [30], is to determine whether there is an HB threshold for τ for the synchronous mode along the upper solution branch when $S_0 > S_{0c}$. For this range of S_0, we recall that the asynchronous mode is linearly stable.

To study this question, we numerically seek a parameterization of any HB threshold in the form $\tau = \tau_H(\lambda_I)$ and $S_0 = S_0(\lambda_I)$, which implicitly yields $\tau = \tau_H(S_0)$. By setting $g(i\lambda_I) = 0$ in (2.5), we obtain from (2.21) with χ_s the complex-valued equation

$$\frac{S_0^2(1+\mu+i\tau\lambda_I)+b(1+i\tau\lambda_I)}{2S_0^2(1+\mu+i\tau\lambda_I)} = \mathcal{F}_R(\lambda_I) + i\mathcal{F}_I(\lambda_I)\,, \tag{2.23}$$

which yields

$$1+\mu+\frac{b}{S_0^2} = 2(1+\mu)\mathcal{F}_R - 2\tau\lambda_I\mathcal{F}_I\,, \qquad \tau\lambda_I\left(\frac{b}{S_0^2}+1\right) = 2\mathcal{F}_I(1+\mu) + 2\tau\lambda_I\mathcal{F}_R\,.$$

By eliminating $\tau\lambda_I$, we obtain a quadratic equation for b/S_0^2, which has two possible roots. After some algebraic simplification we obtain that

$$\tau_H = \frac{1}{4\lambda_I\mathcal{F}_I}\left[\mu\left(2\mathcal{F}_R-1\right) \mp \sqrt{\mu^2\left(2\mathcal{F}_R-1\right)^2 - 16\mathcal{F}_I^2(1+\mu)}\right]\,, \tag{2.24a}$$

$$S_0 = \sqrt{b}\left[\left(2\mathcal{F}_R-1\right)\left(1+\frac{\mu}{2}\right) \pm \frac{1}{2}\sqrt{\mu^2\left(2\mathcal{F}_R-1\right)^2 - 16\mathcal{F}_I^2(1+\mu)}\right]^{-1/2}\,. \tag{2.24b}$$

By sweeping in λ_I and using (2.24), in Figure 4 we plot the HB threshold τ_H and corresponding eigenvalue λ_{IH} versus S_0 for a fixed value $\mu = 2$. Our results show that a unique HB threshold occurs for the synchronous mode only on the middle (dashed) branch of the bifurcation curve in Figure 3 for which $S_{0f} < S_0 < S_{0c}$. There is no HB value of τ for the synchronous mode on the upper branch where $S_0 > S_{0c}$. As a remark, in our sweep in λ_I using (2.24), both choices of the sign in (2.24) were needed to cover the full range $S_{0f} < S_0 < S_{0c}$ with the discriminant of the square root vanishing at the intermediate value $\lambda_I \approx 0.4962$ when $\mu = 2$.

Finally, we use (2.24) to determine the limiting behavior as $S_0 \to S_{0f}^+$ and as $S_0 \to S_{0c}^-$ of the HB threshold τ_H, as observed in Figure 4(a). To calculate the limiting behavior of τ_H as $S_0 \to S_{0f}^+$, we substitute the local behavior for $\mathcal{F}_R$ and $\mathcal{F}_I$ as $\lambda_I \to 0$ from (2.7b) into (2.24a) and choose the minus sign. Then, by using the asymptotic estimate $x - \sqrt{x^2-h} \sim h/(2x)$

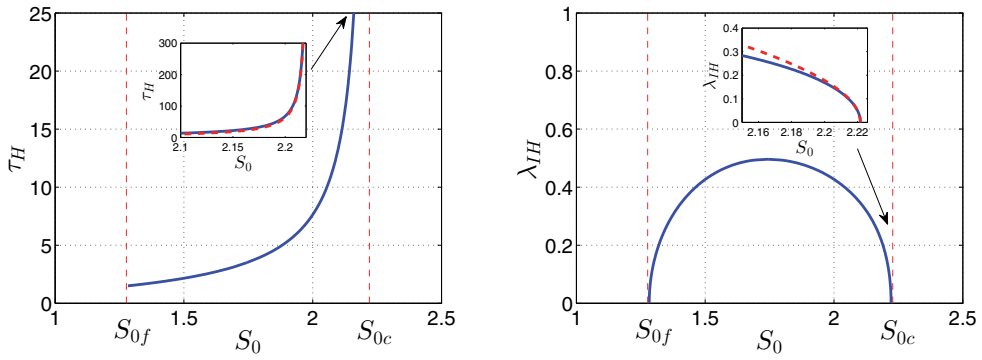

(a) τ_H versus S_0 (b) λ_{IH} versus S_0

Figure 4. *Plot of the HB threshold τ_H (left panel) and imaginary eigenvalue λ_{IH} (right panel) versus S_0 for the synchronous mode of instability for the GS model on the interval $S_{0f} < S_0 < S_{0c}$ when $\mu = 2$, as obtained from (2.24). There is no HB threshold for $S_0 > S_{0c}$, and $\tau_H \to +\infty$ while $\lambda_{IH} \to 0^+$ as $S_0 \to S_{0c}^-$. The asymptotic results given in (2.25b) (dashed curves) for τ_H and λ_{IH} as $S_0 \to S_{0c}^-$ shown in the two inserts agree well with the numerical results from (2.24).*

for $h \ll 1$ and $x > 0$ with $x = \mathcal{O}(1)$, we obtain

$$\tau_H = \lim_{\lambda_I \to 0} \frac{1}{2\lambda_I^2} \left[\mu \left(1 - 2\kappa_c \lambda_I^2\right) - \sqrt{\mu^2 \left(1 - 2\kappa_c \lambda_I^2\right)^2 - 4\lambda_I^2 (1+\mu)} \right]$$
$$= \lim_{\lambda_I \to 0} \frac{1}{2\lambda_I^2} \left[\frac{4\lambda_I^2 (1+\mu)}{2\mu \left(1 - 2\kappa_c \lambda_I^2\right)} \right] .$$

This yields that

$$\tau_H \to \frac{(1+\mu)}{\mu} , \qquad \text{as} \qquad S_0 \to S_{0f}^+ \equiv \sqrt{\frac{b}{1+\mu}} . \tag{2.25a}$$

For $\mu = 2$, this yields $\tau_H \to 1.5$ as $S_0 \to S_{0f}^+$ and is consistent with the results in Figure 4(a). Next, we consider the limiting behavior for τ_H and λ_{IH} as $S_0 \to S_{0c}^-$. We use the local behavior for $\mathcal{F}_R$ and $\mathcal{F}_I$ as $\lambda_I \to 0$ in (2.24b) with the plus sign and in (2.24a) with the minus sign. This leads to $b/S_0^2 \sim 1 + \lambda_I^2 \left(1 - 2\kappa_c + \mu^{-1}\right)$ and $\tau_H \sim \mu/\lambda_I^2$. This yields the limiting behavior

$$\lambda_{IH} \sim \sqrt{\frac{b - S_0^2}{S_0^2 \left(1 - 2\kappa_c + \mu^{-1}\right)}} , \qquad \tau_H \sim \frac{S_0^2 \left[1 + \mu(1 - 2\kappa_c)\right]}{b - S_0^2} , \quad \text{as} \quad S_0 \to S_{0c}^- . \tag{2.25b}$$

In the inserts of Figure 4, this limiting behavior in (2.25b) is favorably compared with numerical results computed from the parameterization (2.24).

3. Anomalous scaling of the Hopf bifurcation threshold. The central result of section 2 for the GM, Schnakenberg, and GS models is that, for the range $D = D_0/\nu$ and $\tau = \mathcal{O}(1)$, there is no synchronous oscillatory instability of the spot amplitudes for an N-spot quasi-equilibrium pattern in the parameter range where the asynchronous mode is linearly stable.

However, the key limitation on the NLEP analysis in section 2 is that the bilinear multiplier χ in (2.1) is valid only under the assumption that $D = \mathcal{O}(\nu^{-1})$ and $\tau = \mathcal{O}(1)$. Since the HB threshold τ_H was found in section 2 to become unbounded at the edge of the instability threshold for the asynchronous mode, this suggests that we need to rederive the appropriate form of the NLEP and its multiplier for the case where τ can be asymptotically large as $\varepsilon \to 0$. By studying this modified NLEP problem we will show that there is an HB theshold τ_H, for which $\tau_H \to \infty$ as $\varepsilon \to 0$, in the parameter range where the asynchronous mode is linearly stable.

3.1. The Gierer–Meinhardt model. As shown in Appendix C, the modified NLEP problem for $\Psi = \Psi(\rho)$, valid for $D = D_0/\nu$ and arbitrary τ, is

$$L_0\Psi - \sigma_j(\lambda) w^2 \frac{\int_0^\infty w\Psi\rho\, d\rho}{\int_0^\infty w^2\rho\, d\rho} = \lambda\Psi\,, \qquad \Psi \to 0 \quad \text{as} \quad \rho \to \infty\,, \tag{3.1a}$$

where the local operator L_0 is defined in (1.4b), and where $w(\rho)$ is the ground-state solution satisfying (1.4c). In (3.1a), there are N choices of the multiplier $\sigma_j(\lambda)$, given by

$$\sigma_j(\lambda) = \frac{2}{1+\mu}\left(1 + 2\pi\nu\kappa_{\lambda,j}\right)\,, \qquad j = 1,\dots,N\,; \qquad \mu \equiv \frac{2\pi N D_0}{|\Omega|}\,. \tag{3.1b}$$

Here $D = D_0/\nu$ and $\kappa_{\lambda,j}$ are the eigenvalues of the λ-dependent Green's matrix $\mathcal{G}_\lambda$ given by

$$\mathcal{G}_\lambda \mathbf{v}_j = \kappa_{\lambda,j}\mathbf{v}_j\,, \qquad j = 1,\dots,N\,. \tag{3.2}$$

The entries of this Green's matrix are obtained from the reduced-wave Green's function $G_\lambda(\mathbf{x};\mathbf{x}_i)$, defined by

$$\Delta G_\lambda - \theta_\lambda^2 G_\lambda = -\delta(\mathbf{x}-\mathbf{x}_i)\,, \quad \mathbf{x}\in\Omega\,; \qquad \partial_n G_\lambda = 0\,, \quad \mathbf{x}\in\partial\Omega\,, \tag{3.3a}$$

$$G_\lambda(\mathbf{x};\mathbf{x}_i) = -\frac{1}{2\pi}\log|\mathbf{x}-\mathbf{x}_i| + R_{\lambda,i} + o(1)\,, \quad \text{as} \quad \mathbf{x}\to\mathbf{x}_i\,, \tag{3.3b}$$

where $R_{\lambda,i}$ is the regular part of $G_\lambda(\mathbf{x};\mathbf{x}_i)$ at $\mathbf{x} = \mathbf{x}_i$. Here $\theta_\lambda^2 \equiv \nu(1+\tau\lambda)/D_0$. In (3.2), and in terms of the spatial configuration $\mathbf{x}_1,\dots,\mathbf{x}_N$ of the localized spots, the entries of the symmetric $N\times N$ Green's matrix $\mathcal{G}_\lambda$ are

$$(\mathcal{G}_\lambda)_{ij} = G_\lambda(\mathbf{x}_j;\mathbf{x}_i)\,, \quad i\neq j\,; \qquad (\mathcal{G}_\lambda)_{jj} = R_{\lambda,j}\,. \tag{3.4}$$

We first show how to recover the NLEP for the GM model given by (1.4a), where the two multipliers are given in (2.11). For $\tau = \mathcal{O}(1)$, we readily calculate from (3.3) that for $\nu \ll 1$

$$G_\lambda = \frac{D_0}{\nu(1+\tau\lambda)|\Omega|} + G_0 + \mathcal{O}(\nu)\,, \qquad R_\lambda = \frac{D_0}{\nu(1+\tau\lambda)|\Omega|} + R_0 + \mathcal{O}(\nu)\,, \tag{3.5}$$

where G_0 is the Neumann Green's function with regular part R_0, satisfying (A.4). Thus, for $\nu \ll 1$, the Green's matrix $\mathcal{G}_\lambda$ is

$$\mathcal{G}_\lambda = \frac{D_0 N}{\nu(1+\tau\lambda)|\Omega|}E + \mathcal{G}_0 + \mathcal{O}(\nu)\,, \qquad E = \frac{1}{N}\mathbf{e}\mathbf{e}^T\,, \tag{3.6}$$

where $\mathbf{e} = (1, \dots, 1)^T$. Now since $E\mathbf{e} = \mathbf{e}$ and $E\mathbf{q}_j = 0$ for $j = 2, \dots, N$, where $\mathbf{q}_j^T\mathbf{e} = 0$, the eigenvalues $\kappa_{\lambda,j}$ of $\mathcal{G}_\lambda$ are $\kappa_{\lambda,1} \sim D_0 N/\left[\nu(1+\tau\lambda)|\Omega|\right]$ and $\kappa_{\lambda,j} = \mathcal{O}(1)$ for $j = 2, \dots, N$. In this way, we get

$$2\pi\nu\kappa_{\lambda,1} \sim \frac{\mu}{1+\tau\lambda}\,; \qquad 2\pi\nu\kappa_{\lambda,j} = \mathcal{O}(\nu) \quad \text{for} \quad j = 2, \dots, N\,. \tag{3.7}$$

Upon substituting (3.7) into (3.1b) we recover the multipliers for the synchronous and asynchronous modes given in (2.11) for the case where $D = D_0/\nu$ and $\tau = \mathcal{O}(1)$. In this parameter regime, the $N-1$ modes $\mathbf{v}_j = \mathbf{q}_j$ for $j = 2, \dots, N$, correspond to asynchronous perturbations in the spot amplitudes, which conserve the sum of the spot amplitudes via $\mathbf{q}_j^T\mathbf{e} = 0$, while $\mathbf{v}_1 = \mathbf{e}$ is the mode for which this perturbation is synchronous.

Our main focus here is to consider the new limit where $\tau \gg 1$ so that $|(1+\tau\lambda)\nu/D_0| \gg 1$ in (3.3). In this limit, $G_\lambda(\mathbf{x};\mathbf{x}_i)$ decays rapidly away from $\mathbf{x}_i$ so that, except within a thin boundary layer near $\partial\Omega$, we have

$$G_\lambda(\mathbf{x};\mathbf{x}_i) \sim \frac{1}{2\pi} K_0\left(\theta_\lambda|\mathbf{x}-\mathbf{x}_i|\right)\,, \qquad \theta_\lambda \equiv \sqrt{\frac{(1+\tau\lambda)\nu}{D_0}}\,. \tag{3.8}$$

Here we must specify the principal branch of the square root so that $G_\lambda(\mathbf{x};\mathbf{x}_i)$ decays exponentially away from $\mathbf{x}_i$. By using the well-known behavior $K_0(z) \sim -\log z + \log 2 - \gamma + \mathcal{O}(z^2\log z)$, where $\gamma \approx 0.57721\dots$ is Euler's constant, we calculate that the regular part of (3.8) is independent of $\mathbf{x}_i$, and as $\mathbf{x} \to \mathbf{x}_i$

$$G_\lambda(\mathbf{x};\mathbf{x}_i) \sim -\frac{1}{2\pi}\log|\mathbf{x}-\mathbf{x}_i| + R_\lambda\,; \quad R_\lambda \equiv \frac{1}{2\pi}\left(-\frac{1}{2}\log\left(\nu(1+\tau\lambda)\right) + \log\left(2\sqrt{D_0}\right) - \gamma\right)\,. \tag{3.9}$$

When $|\theta_\lambda| \gg 1$, the off-diagonal entries of the Green's matrix are exponentially small and satisfy

$$\left(\mathcal{G}_\lambda\right)_{i,j} = \mathcal{O}\left(|\mathbf{x}_i-\mathbf{x}_j|^{-1/2}e^{-\theta_\lambda|\mathbf{x}_i-\mathbf{x}_j|}\right) \ll 1 \quad \text{for} \quad |\mathbf{x}_i-\mathbf{x}_j| = \mathcal{O}(1)\,, \tag{3.10}$$

since $\mathrm{Re}(\theta_\lambda) > 0$. Therefore, when $|\theta_\lambda| \gg 1$, we have that $\mathcal{G}_\lambda$ is, asymptotically, a multiple of the identity, given by $\mathcal{G}_\lambda \sim R_\lambda I$. As a result, the eigenvalues of $\mathcal{G}_\lambda$ in (3.2) are, asymptotically, the common value $\kappa_{\lambda,j} \sim R_\lambda$ for $j = 1, \dots, N$. We remark that in this regime where $|\theta_\lambda| \gg 1$, the temporal oscillations of the spot amplitudes can no longer be classified as being either synchronous or asynchronous. In fact, since $\mathcal{G}_\lambda$ is, asymptotically, a multiple of the identity, the perturbations of the spot amplitudes, characterized by the vectors $\mathbf{v}_j$ for $j = 1, \dots, N$, now span all of $\mathbb{R}^N$.

A key observation is that in order to make $\nu\kappa_{\lambda,j} = \mathcal{O}(1)$ in the multiplier (3.1b) of the NLEP (3.1a) we need to allow for $\tau \gg 1$ and introduce a rescaling of this parameter in terms of ε. This is done by defining a new parameter $\tau_c > 0$ via

$$\tau \equiv \frac{\varepsilon^{-\tau_c}}{\nu}\,, \qquad \tau_c > 0\,. \tag{3.11}$$

When $\tau_c > 0$, we have $\tau \gg 1$, with the scaling being *anomalous in* ε. However, from the self-consistency condition of (A.11) of Appendix A we require that $\varepsilon^2\tau\lambda/D \ll 1$. With (3.11) and $D = D_0/\nu$, this requirement is satisfied provided that τ_c is not too large, i.e., that

$$\frac{\varepsilon^{2-\tau_c}\lambda}{D_0} \ll 1\,. \tag{3.12}$$

By combining (3.11) with (3.9), we calculate that

$$2\pi\nu\kappa_{\lambda,j} = -\frac{\tau_c}{2} + \nu\mathcal{K}_\varepsilon\,, \qquad \mathcal{K}_\varepsilon \equiv -\frac{1}{2}\log\left(\lambda + \nu\varepsilon^{\tau_c}\right) + \log\left(2\sqrt{D_0}\right) - \gamma\,, \tag{3.13}$$

so that the N multipliers in (3.1b) collapse to a common multiplier when $|\theta_\lambda| \gg 1$, given by

$$\sigma_j(\lambda) = \sigma_{\rm gm}(\lambda) \equiv \frac{2}{1+\mu}\left(1 - \frac{\tau_c}{2} + \nu\mathcal{K}_\varepsilon\right)\,. \tag{3.14}$$

The discrete eigenvalues of the modified NLEP (3.1a) with multiplier (3.14) are the roots λ of $g_{\rm gm}(\lambda) = 0$, where

$$g_{\rm gm}(\lambda) \equiv \frac{(1+\mu)}{2}\left(1 - \frac{\tau_c}{2} + \nu\mathcal{K}_\varepsilon\right)^{-1} - \mathcal{F}(\lambda)\,, \qquad \mathcal{F}(\lambda) \equiv \frac{\int_0^\infty w\left[(L_0-\lambda)^{-1}w^2\right]\rho\,d\rho}{\int_0^\infty w^2\rho\,d\rho}\,. \tag{3.15}$$

We now determine an HB threshold value of τ_c for the modified NLEP (3.1a) with multiplier $\sigma_{\rm gm}$ in (3.14), by examining whether $g_{\rm gm}(\lambda) = 0$ in (3.15) can have any purely complex conjugate roots. To motivate the analysis below we first neglect $\nu\mathcal{K}_\varepsilon$ in (3.15) and readily conclude from Lemmas 2.1 and 2.2 that $\mathrm{Re}(\lambda) < 0$ iff $\sigma_{\rm gm} > 1$, which holds when $\tau_c < 1-\mu$. When $\tau_c = 1-\mu$, we have $\lambda = 0$. We observe that $\tau_c \approx 1-\mu > 0$ on the parameter range $0 < \mu < 1$, where the asynchronous mode in section 2.1 was found to be linearly stable and where the synchronous mode had no HB threshold when $\tau = \mathcal{O}(1)$.

With this motivation, we fix μ in $0 < \mu < 1$ and use (3.15) to determine an HB threshold where τ_c is near the critical value $1-\mu$ and where $\lambda = i\lambda_I$ satisfies $0 < \lambda_I \ll 1$. To do so, we first separate (3.15) into real and imaginary parts to get

$$\tau_c - (1-\mu) = (\tau_c - 2)\left[1 - \mathrm{Re}(\mathcal{F}(i\lambda_I))\right] + 2\nu\mathrm{Re}\left[\mathcal{K}_\varepsilon\mathcal{F}(i\lambda_I)\right]\,, \tag{3.16a}$$

$$(\tau_c - 2)\lambda_I = 4\nu\mathrm{Im}\left[\mathcal{K}_\varepsilon\mathcal{F}(i\lambda_I)\right]\,, \tag{3.16b}$$

where $\mathcal{K}_\varepsilon$ is defined in (3.13). In (3.16) we then use (2.7) to express the local behavior of $\mathcal{F}(i\lambda_I)$ as

$$\mathcal{F}(i\lambda_I) \sim 1 + \frac{i\lambda_I}{2} - \kappa_c\lambda_I^2 + \cdots \qquad \text{for} \quad \lambda_I \ll 1\,, \tag{3.17}$$

where κ_c is defined in (2.7c). By using (3.17), we will show for $\nu \ll 1$ that (3.16) has a root with $\tau_c \sim (1-\mu) - \nu\log\nu + \cdots$ and $\lambda_I = \mathcal{O}(\nu)$. For $0 < \mu < 1$, so that $\tau_c > 0$, and with $\lambda_I = \mathcal{O}(\nu)$, we estimate from (3.13) that

$$\mathcal{K}_\varepsilon = \mathcal{K}_0 + \mathcal{O}(\nu\varepsilon^{\tau_c})\,, \quad \text{where} \quad \mathcal{K}_0 = -\frac{i\pi}{4} - \frac{1}{2}\log\lambda_I + \beta_k\,, \quad \beta_k \equiv \log\left(2\sqrt{D_0}\right) - \gamma\,. \tag{3.18}$$

Therefore, in (3.13) and in (3.16) we can replace $\mathcal{K}_\varepsilon$ with $\mathcal{K}_0$ when $\tau_c > 0$.

By asymptotically calculating the root of (3.16) with (3.17) and (3.18) when $\nu \ll 1$, we obtain the following main asymptotic result characterizing the HB threshold for a multispot pattern for the GM model (1.1) in the regime where $D = D_0/\nu$ and $\mu = 2\pi N D_0/|\Omega| < 1$.

Proposition 3.1. *Consider an N-spot quasi-equilibrium pattern for the GM model (1.1) in the regime where $D = D_0/\nu$ with $\nu \ll 1$. Define $\mu \equiv 2\pi N D_0/|\Omega|$ and suppose that $0 < \mu < 1$. Then, the modified NLEP (3.1) has a Hopf bifurcation, corresponding to temporal oscillations in the spot amplitudes, when $\tau = \tau_H \gg 1$ and $\lambda = \pm i\lambda_I$, where $\lambda_I \ll 1$. For $\nu \ll 1$, the asymptotic expansion of this HB threshold and Hopf frequency is given by*

$$\tau_H \sim \frac{1}{\nu}\varepsilon^{-\tau_c}\,, \quad \tau_c = (1-\mu) - \nu\log\nu + \tau_{c1}\nu + \tau_{c2}\nu^2 + \cdots\,; \quad \lambda \sim i\nu\left(\lambda_{I0} + \nu^2\lambda_{I2} + \cdots\right)\,, \tag{3.19}$$

where the coefficients in this expansion are defined by

$$\tau_{c1} = 2\beta_k - \log\lambda_{I0}\,, \quad \tau_{c2} = \frac{\pi^2}{4(1+\mu)}(1-4\kappa_c)\,, \quad \lambda_{I0} = \frac{\pi}{(1+\mu)}\,, \quad \lambda_{I2} = \frac{\pi^3}{(1+\mu)^3}\left(\frac{1}{4} - 2\kappa_c\right)\,. \tag{3.20}$$

Here β_k and κ_c are defined in (3.18) and (2.7c), respectively.

Proof. We substitute (3.17) and (3.18) into (3.16), and use $\mathrm{Re}(z_1 z_2) = \mathrm{Re}(z_1)\mathrm{Re}(z_2) - \mathrm{Im}(z_1)\mathrm{Im}(z_2)$ together with $\mathrm{Im}(z_1 z_2) = \mathrm{Re}(z_1)\mathrm{Im}(z_2) + \mathrm{Re}(z_2)\mathrm{Im}(z_1)$, to get

$$\tau_c - (1-\mu) \sim (\tau_c - 2)\kappa_c\lambda_I^2 + 2\nu\mathrm{Re}(\mathcal{K}_0)(1-\kappa_c\lambda_I^2) - \mathrm{Im}(\mathcal{K}_0)\nu\lambda_I\,, \tag{3.21a}$$

$$(\tau_c - 2)\lambda_I \sim 4\nu\left[\frac{\lambda_I}{2}\mathrm{Re}(\mathcal{K}_0) + \mathrm{Im}(\mathcal{K}_0)(1-\kappa_c\lambda_I^2)\right]\,, \tag{3.21b}$$

where we calculate from (3.18) that $\mathrm{Im}(\mathcal{K}_0) = -\pi/4$ and $\mathrm{Re}(\mathcal{K}_0) = \beta_k - \frac{1}{2}\log\lambda_I$. Then, since $\lambda_I \ll 1$, from the first and second equations in (3.21) we get $\tau_c \sim 1-\mu$ and $(\tau_c - 2)\lambda_I \sim 4\nu\mathrm{Im}(\mathcal{K}_0)$, respectively. This second expression yields $\lambda_I \sim \nu\pi/(1+\mu)$.

To systematically determine the higher order correction terms we write $\lambda_I = \nu\tilde{\lambda}_I$, so that (3.21) becomes

$$\tau_c - (1-\mu) = -\nu\log\nu - \nu\log\tilde{\lambda}_I + 2\nu\beta_k + (\tau_c - 2)\kappa_c\nu^2\tilde{\lambda}_I^2 + \frac{\pi}{4}\nu^2\tilde{\lambda}_I + \mathcal{O}(\nu^3\log\nu)\,, \tag{3.22a}$$

$$(\tau_c - 2)\tilde{\lambda}_I = -\pi + \tilde{\lambda}_I\left[-\nu\log\nu - \nu\log\tilde{\lambda}_I + 2\nu\beta_k\right] + \pi\kappa_c\tilde{\lambda}_I^2\nu^2 + \cdots\,. \tag{3.22b}$$

Now define $\tau_{c0} \equiv 1-\mu$ and $\lambda_{I0} \equiv \pi/(1+\mu)$. From (3.22a) we get $\tau_c = \tau_{c0} - \nu\log\nu + \mathcal{O}(\nu)$. Next, we expand τ_c as in (3.19) and $\tilde{\lambda}_I$ as $\tilde{\lambda}_I = \lambda_{I0} + \nu\lambda_{I1} + \nu^2\lambda_{I2} + \cdots$ and substitute into (3.22). By comparing the $\mathcal{O}(\nu)$ terms in (3.22a) we get that $\tau_{c1} = 2\beta_k - \log\lambda_{I0}$. From the $\mathcal{O}(\nu)$ terms in (3.22b), we conclude that $(\tau_{c0} - 2)\lambda_{I1} = \lambda_{I0}(2\beta_k - \log\lambda_{I0} - \tau_{c1})$. By using our expression for τ_{c1} we get that $\lambda_{I1} = 0$. Then, by using $\log\tilde{\lambda}_I = \log\tilde{\lambda}_{I0} + \mathcal{O}(\nu^2)$, we obtain from the $\mathcal{O}(\nu^2)$ terms in (3.22) that τ_{c2} and λ_{I2} satisfy

$$(\tau_{c0} - 2)\,\lambda_{I2} + \tau_{c2}\lambda_{I0} = \pi\kappa_c\lambda_{I0}^2\,, \qquad \tau_{c2} = (\tau_{c0} - 2)\kappa_c\lambda_{I0}^2 + \frac{\pi}{4}\lambda_{I0}\,.$$

This determines τ_{c2} and λ_{I2} as written in (3.20). This completes the derivation of (3.19). ∎

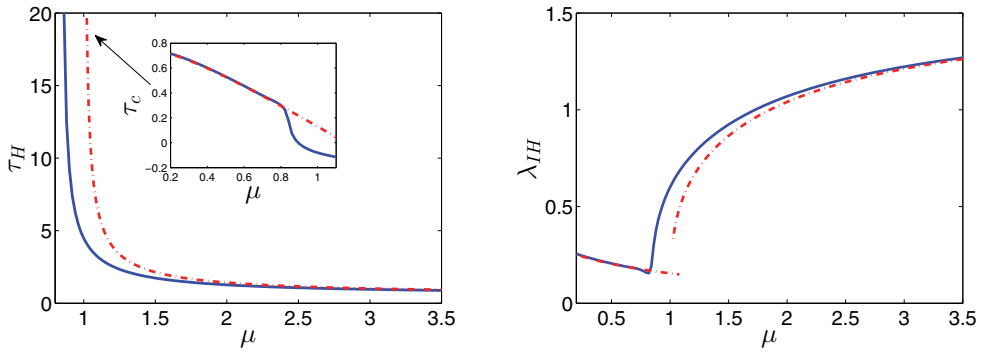

(a) τ_H versus μ (b) λ_{IH} versus μ

Figure 5. *Left panel: HB threshold τ_H (solid curve) versus μ for a one-spot solution to the GM model (1.1) centered at the origin of the unit disk with $\nu = 0.1$, as computed from (3.23). The dot-dashed curve is the HB threshold for the NLEP bilinear multiplier, obtained from (2.13). In the insert, $\tau_c \equiv \nu \log(\tau_H \nu)$, as computed from (3.23), is seen to compare well with the asymptotic result in (3.19) on $\mu < 1$, except near $\mu = 1$. Right panel: λ_{IH} versus μ from (3.23) (solid curve), from the NLEP theory with bilinear multiplier from (2.13) (dot-dashed curve for $\mu > 1$), and from the asymptotic result in (3.19) (dot-dashed curve for $\mu < 1$).*

We now make a few remarks regarding this main result. We first observe that since $0 < \mu < 1$, our scaling threshold for τ_c and λ_I satisfies the required consistency condition (3.12) for any $0 < \mu < 1$. Second, since $\lambda_I \ll 1$, the temporal oscillations of the spot amplitudes for the Hopf bifurcation are of low frequency. Next, we observe that in the regime where $\tau \gg 1$ the HB threshold for the spot amplitudes is, asymptotically, independent of the spatial configuration of the spots and depends only on the number of spots. This qualitative feature that the HB threshold is independent of the spot locations was also found to hold for the conventional NLEP analysis in section 2.1 for the regime where $D = D_0/\nu$ and $\tau = \mathcal{O}(1)$. Finally, our analysis of the anomalous HB threshold in the regime where $0 < \mu < 1$ is not uniformly valid in the limit $\mu \to 1^-$ where $\tau_c \to 0^+$. When $|\mu - 1| \ll 1$, we will show in section 4 that the spatial configuration of the spots is important for determining the HB threshold.

In Figure 5 we illustrate our main result for the HB threshold and eigenvalue for the special case of a one-spot solution centered at the origin of the unit disk with $\nu = 0.1$. From the modified NLEP (3.1), and by calculating the reduced-wave Green's function (3.3) analytically, the HB threshold τ_H and λ_{IH} is the root of

$$\text{(3.23a)} \qquad \mathrm{Re}(\kappa_{\lambda,1}) + \frac{1}{2\pi\nu}\left(1 - \frac{(1+\mu)\mathcal{F}_R}{2\left(\mathcal{F}_R^2 + \mathcal{F}_I^2\right)}\right) = 0\,, \qquad \mathrm{Im}(\kappa_{\lambda,1}) + \frac{1}{4\pi\nu}\frac{(1+\mu)\mathcal{F}_I}{\left(\mathcal{F}_R^2 + \mathcal{F}_I^2\right)} = 0\,,$$

where $\kappa_{\lambda_1} \equiv R_{\lambda,1}$ is given explicitly in terms of modified Bessel functions as

$$\text{(3.23b)} \qquad R_{\lambda,1} = \frac{1}{2\pi}\left[-\frac{1}{2}\log\left(\nu(1+\tau\lambda)\right) + \log\left(2\sqrt{D_0}\right) - \gamma\right] - \frac{1}{2\pi}\frac{K_0'(\theta_\lambda)}{I_0'(\theta_\lambda)}\,, \qquad \theta_\lambda \equiv \sqrt{\frac{\nu\left(1 + i\tau\lambda_{IH}\right)}{D_0}}\,,$$

where γ is Euler's constant. We remark that the term in (3.23b) involving modified Bessel functions represents the effect of the finite domain. In Figure 5 we compare the HB threshold

and eigenvalue as computed from (3.23), from the NLEP theory with bilinear multiplier in (2.13) on $\mu > 1$, and from the new asymptotic scaling law in (3.19) valid on $\mu < 1$. We observe from this figure that this new scaling law accurately determines the HB threshold and eigenvalue on $0 < \mu < 1$, except near $\mu = 1$.

3.2. The Schnakenberg model. An analysis similar to that in section 3.2 can be done for the Schnakenberg model (1.3). As shown in Appendix A, the modified NLEP problem, valid for $D = D_0/\nu$ and for arbitrary τ, is (3.1a), where the N choices for the multiplier of the NLEP are

$$\sigma_j(\lambda) = \frac{2\,(1 + 2\pi\nu\kappa_{\lambda,j})}{1 + \alpha + 2\pi\nu\kappa_{\lambda,j}}\,, \qquad j = 1, \ldots, N\,; \qquad \alpha \equiv \frac{4\pi^2 b D_0 N^2}{|\Omega|^2 \mathcal{A}^2}\,. \tag{3.24}$$

Here $|\Omega|$ is the area of Ω, and $b \equiv \int_0^\infty \rho w^2\, d\rho \approx 4.935$, where $w(\rho)$ is the ground-state satisfying (1.4c).

In (3.24), the $\kappa_{\lambda,j}$ for $j = 1, \ldots, N$ are the eigenvalues of the Green's matrix in (3.4), where the entries of this Green's matrix are now defined in terms of the Green's function $G_\lambda(\mathbf{x}; \mathbf{x}_i)$ satisfying

$$\Delta G_\lambda - \frac{\nu\tau\lambda}{D_0} G_\lambda = -\delta(\mathbf{x} - \mathbf{x}_i)\,, \quad \mathbf{x} \in \Omega\,; \qquad \partial_n G_\lambda = 0\,, \quad \mathbf{x} \in \partial\Omega\,, \tag{3.25a}$$

$$G_\lambda(\mathbf{x}; \mathbf{x}_i) = -\frac{1}{2\pi} \log|\mathbf{x} - \mathbf{x}_i| + R_{\lambda,i} + o(1)\,, \quad \text{as} \quad \mathbf{x} \to \mathbf{x}_i\,. \tag{3.25b}$$

We recall from the conventional NLEP analysis in section 2.2 for the regime where $D = D_0/\nu$ and $\tau = \mathcal{O}(1)$ that, for any fixed $\mu > 0$ and $\alpha < 1$, the asynchronous mode is linearly stable while the synchronous mode is also linearly stable for any $\tau > 0$. We showed that the synchronous mode does undergo a Hopf bifurcation when $\alpha > 1$, with the HB threshold value of τ tending to infinity and the corresponding HB frequency tending to zero as $\alpha \to 1^+$. By analyzing the modified NLEP (3.1) with multiplier (3.24), we will show that there is an HB threshold τ_H in the regime where $\alpha < 1$ with $\tau_H \to +\infty$ as $\varepsilon \to 0$.

We use the same approach as in section 3.1. We assume that $|\tau\lambda\nu/D_0| \gg 1$ so that $G_\lambda(\mathbf{x}; \mathbf{x}_i) \sim \frac{1}{2\pi} K_0\left(\omega_\lambda |\mathbf{x} - \mathbf{x}_i|\right)$, where ω_λ is the principal branch of $\omega_\lambda \equiv \sqrt{\tau\lambda\nu/D_0}$. When $|\mathbf{x}_i - \mathbf{x}_j| = \mathcal{O}(1)$ for $i \neq j$, we get $\mathcal{G}_\lambda \sim R_\lambda I$, where R_λ is given in (3.9) upon replacing $(1+\tau\lambda)$ with $\tau\lambda$. Then, upon introducing the scaling law $\tau = \nu^{-1}\varepsilon^{-\tau_c}$, we obtain that

$$2\pi\nu\kappa_{\lambda,j} = -\frac{\tau_c}{2} + \nu\mathcal{K}_0\,, \qquad \mathcal{K}_0 \equiv -\frac{1}{2}\log\lambda + \beta_k\,, \qquad \beta_k \equiv \log\left(2\sqrt{D_0}\right) - \gamma\,, \tag{3.26}$$

where γ is Euler's constant. Therefore, when $\tau \gg 1$, the N multipliers in (3.24) collapse to a common multiplier

$$\sigma_j(\lambda) = \sigma_{\rm sc}(\lambda) \equiv \frac{2\,(1 - \tau_c/2 + \nu\mathcal{K}_0)}{(1 + \alpha - \tau_c/2 + \nu\mathcal{K}_0)}\,. \tag{3.27}$$

The discrete eigenvalues of the modified NLEP (3.1a) with multiplier (3.27) are the roots of $g_{\rm sc}(\lambda) = 0$, where

$$g_{\rm sc}(\lambda) \equiv \frac{(1 + \alpha - \tau_c/2 + \nu\mathcal{K}_0)}{2\,(1 - \tau_c/2 + \nu\mathcal{K}_0)} - \mathcal{F}(\lambda)\,, \qquad \mathcal{F}(\lambda) \equiv \frac{\int_0^\infty w\left[(L_0 - \lambda)^{-1} w^2\right]\rho\, d\rho}{\int_0^\infty w^2 \rho\, d\rho}\,. \tag{3.28}$$

We now examine whether (3.28) can have any purely complex conjugate roots. If we neglect $\nu\mathcal{K}_0$ in (3.28), we conclude from Lemmas 2.1 and 2.2 that $\mathrm{Re}(\lambda) < 0$ iff $\sigma_c > 1$, which holds when $\tau_c < 2(1-\alpha)$. When $\tau_c = 2(1-\alpha)$, we have $\lambda = 0$ is a root of (3.28). Notice that $\tau_c = 2(1-\alpha) > 0$ on the parameter range $0 < \alpha < 1$, where the asynchronous mode in section 2.2 was found to be linearly stable and where the synchronous mode had no HB threshold when $\tau = \mathcal{O}(1)$.

For a fixed α in $0 < \alpha < 1$ the asymptotic analysis to characterize the HB threshold and frequency when τ_c is near the critical value $2(1-\alpha)$ parallels that in section 3.1. We let $\lambda = i\lambda_I$ and upon setting $g_{\rm sc}(i\lambda_I) = 0$ in (3.28), we obtain that

$$1 + \alpha - \frac{\tau_c}{2} - (2-\tau_c)\mathcal{F}(i\lambda_I) = \nu\mathcal{K}_0\left[2\mathcal{F}(i\lambda_I) - 1\right]. \tag{3.29}$$

We then substitute the local behavior (3.17) for $\mathcal{F}(i\lambda_I)$ into (3.29) and take real and imaginary parts of the resulting expression. This yields that

$$\alpha - 1 + \frac{\tau_c}{2} + (2-\tau_c)\kappa_c\lambda_I^2 \sim \nu\mathrm{Re}(\mathcal{K}_0)\left(1 - 2\kappa_c\lambda_I^2\right) - \nu\lambda_I\mathrm{Im}(\mathcal{K}_0), \tag{3.30a}$$

$$\left(\frac{\tau_c}{2} - 1\right)\lambda_I \sim \nu\mathrm{Im}(\mathcal{K}_0)\left(1 - 2\kappa_c\lambda_I^2\right) + \nu\lambda_I\mathrm{Re}(\mathcal{K}_0), \tag{3.30b}$$

where $\mathrm{Im}(\mathcal{K}_0) = -\pi/4$ and $\mathrm{Re}(\mathcal{K}_0) = \beta_k - \frac{1}{2}\log\lambda_I$. Since $\lambda_I \ll 1$, the leading-order terms in (3.30) are $\tau_c \sim \tau_{c0} \equiv 2(1-\alpha)$ and $(\tau_{c0}/2 - 1)\lambda_I \sim -\nu\pi/4$, which yields $\lambda_I \sim \pi\nu/(4\alpha)$. Since $\lambda_I = \mathcal{O}(\nu)$ and $\tau_{c0} = 2(1-\alpha)$ satisfies $0 < \tau_c < 2$ on $0 < \alpha < 1$, the required consistency condition in (3.12) is always satisfied.

By introducing an asymptotic expansion to systematically calculate the correction terms to this leading-order HB threshold and frequency, as in the proof of Proposition 3.1, we obtain the following main result.

Proposition 3.2. *Consider an N-spot quasi-equilibrium pattern for the Schnakenberg model (1.3) in the regime where $D = D_0/\nu$ with $\nu \ll 1$. Suppose that the feed-rate parameter $\mathcal{A}$ satisfies $\mathcal{A} > \mathcal{A}_c \equiv \frac{2\pi N}{|\Omega|}\sqrt{bD_0}$, where $b \equiv \int_0^\infty \rho w^2\, d\rho \approx 4.935$, and $w(\rho)$ is the ground-state satisfying (1.4c). Then, the modified NLEP (3.1a) with multiplier (3.24) has a Hopf bifurcation, corresponding to temporal oscillations in the spot amplitudes, when $\tau = \tau_H \gg 1$ and $\lambda = \pm i\lambda_I$, where*

$$\tau_H \sim \frac{1}{\nu}\varepsilon^{-\tau_c}, \quad \tau_c = 2(1-\alpha) - \nu\log\nu + \tau_{c1}\nu + \tau_{c2}\nu^2 + \cdots; \quad \lambda \sim i\nu\left(\lambda_{I0} + \nu^2\lambda_{I2} + \cdots\right). \tag{3.31}$$

Here the coefficients are given explicitly by

$$\tau_{c1} = 2\beta_k - \log\lambda_{I0}, \quad \tau_{c2} = \frac{\pi^2}{8\alpha}(1 - 2\kappa_c), \quad \lambda_{I0} = \frac{\pi}{4\alpha}, \quad \lambda_{I2} = \frac{\pi^3}{16\alpha^3}\left(\frac{1}{4} - \kappa_c\right). \tag{3.32}$$

Here α, β_k, and κ_c are defined in (3.24), (3.26), and (2.7c), respectively.

In Figure 6 we plot the HB threshold and eigenvalue for a one-spot solution centered at the origin of the unit disk with $\nu = 0.125$ and $\mu = 2$, for which $D_0 = 1$. In place of (3.23a),

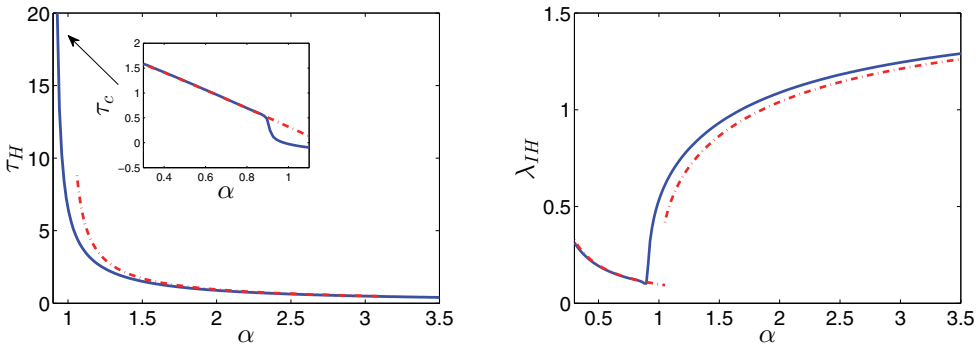

(a) τ_H versus α (b) λ_{IH} versus α

Figure 6. *Left panel: HB threshold τ_H (solid curve) versus α for a one-spot solution to the Schnakenberg model (1.3) centered at the origin of the unit disk with $\nu = 0.125$ and $\mu = 2$, as computed from (3.33). The dot-dashed curve is the HB threshold for the NLEP with a bilinear multiplier (2.18). In the insert, $\tau_c \equiv \nu \log(\tau_H \nu)$ from (3.23) agrees well with the asymptotic result in (3.31) on $\alpha < 1$, except near $\alpha = 1$. Right panel: λ_{IH} versus α from (3.33) (solid curve), from the NLEP with a bilinear multiplier (2.18) (dot-dashed curve for $\alpha > 1$), and from the asymptotic result (3.31) (dot-dashed curve for $\alpha < 1$).*

the HB threshold τ_H and λ_{IH} for the modified NLEP (3.1a) with multiplier (3.24) is the root of

(3.33)
$$\mathrm{Re}(\kappa_{\lambda,1}) + \frac{1}{2\pi\nu}\left(1 + \frac{\alpha\,(1-2\mathcal{F}_R)}{(1-2\mathcal{F}_R)^2 + 4\mathcal{F}_I^2}\right) = 0\,, \qquad \mathrm{Im}(\kappa_{\lambda,1}) + \frac{1}{\pi\nu}\frac{\alpha\mathcal{F}_I}{\left[(1-2\mathcal{F}_R)^2 + 4\mathcal{F}_I^2\right]} = 0\,,$$

where $\kappa_{\lambda_1} \equiv R_{\lambda,1}$ is given in (3.23b), where θ_λ is now defined by $\theta_\lambda \equiv \sqrt{i\nu\tau\lambda_{IH}/D_0}$. In Figure 6 we compare the HB threshold and eigenvalue, as computed from (3.33), with that from the conventional NLEP theory (2.18), valid on $\alpha > 1$, and with that from the new asymptotic scaling law in (3.31), valid on $\alpha < 1$.

3.3. The Gray–Scott model. A similar analysis can be done for the GS model (1.2). As shown in Appendix B, the modified NLEP problem, valid for $D = D_0/\nu$ and for arbitrary τ, is (3.1a), where the N choices for the multiplier of the NLEP are

$$\sigma_j(\lambda) = \frac{2\,(1 + 2\pi\nu\kappa_{\lambda,j})}{1 + b/S_0^2 + 2\pi\nu\kappa_{\lambda,j}}\,, \qquad j = 1, \ldots, N\,. \tag{3.34}$$

Here $|\Omega|$ is the area of Ω, $b \equiv \int_0^\infty \rho w^2\, d\rho \approx 4.935$, where $w(\rho)$ is the ground-state satisfying (1.4c), while S_0 parameterizes the steady-state bifurcation diagram in terms of the feed-rate parameter as in (2.20) (see Figure 3). In (3.34), the $\kappa_{\lambda,j}$ for $j = 1, \ldots, N$ are the eigenvalues of the Green's matrix $\mathcal{G}_\lambda$ in (3.4), where the matrix entries are defined in terms of the reduced-wave Green's function of (3.3).

In our conventional NLEP analysis of section 2.3 for the regime $D = D_0/\nu$ and $\tau = \mathcal{O}(1)$ we showed that on the upper branch of the bifurcation diagram in Figure 3, where $S_0 > S_{0c} \equiv \sqrt{b}$,

the asynchronous mode is linearly stable and the synchronous mode is also linearly stable for any $\tau > 0$. We showed that the synchronous mode does undergo a Hopf bifurcation when $S_{0f} < S_0 < S_{0c}$ (see Figure 3), with the HB threshold value of τ tending to infinity and the corresponding HB frequency tending to zero as $S_0 \to S_{0c}^-$.

We now use the modified NLEP (3.1) with multiplier (3.34) to show that there is an HB threshold τ_H along the upper branch of Figure 3, where $S_0 > S_{0c} \equiv \sqrt{b}$, for which $\tau_H \to +\infty$ as $\varepsilon \to 0$.

We proceed as in sections 3.1 and 3.2. When $\tau \gg \mathcal{O}(\nu^{-1})$, so that $|(1+\tau\lambda)\nu/D_0| \gg 1$, $G_\lambda(\mathbf{x};\mathbf{x}_i)$ is approximated by the free-space Green's function in (3.8) and the Green's matrix $\mathcal{G}_\lambda$ satisfies $\mathcal{G}_\lambda \sim R_\lambda I$, where R_λ is given as in (3.9). We then introduce $\tau_c > 0$ via the scaling law (3.11) and obtain that

$$2\pi\nu\kappa_{\lambda,j} = -\frac{\tau_c}{2} + \nu\mathcal{K}_\varepsilon\,, \qquad \mathcal{K}_\varepsilon \equiv -\frac{1}{2}\log\left(\lambda + \nu\varepsilon^{\tau_c}\right) + \beta_k\,, \qquad \beta_k \equiv \log\left(2\sqrt{D_0}\right) - \gamma\,, \tag{3.35}$$

where γ is Euler's constant. Upon substituting (3.35) into (3.34) we obtain that the N multipliers collapse to a common multiplier given by

$$\sigma_j(\lambda) = \sigma_{\rm gs}(\lambda) \equiv \frac{2\left(1 - \tau_c/2 + \nu\mathcal{K}_\varepsilon\right)}{\left(1 + b/S_0^2 - \tau_c/2 + \nu\mathcal{K}_\varepsilon\right)}\,. \tag{3.36}$$

The discrete eigenvalues of the modified NLEP (3.1a) with multiplier (3.36) are the roots of $g_{\rm gs}(\lambda) = 0$, where

$$g_{\rm gs}(\lambda) \equiv \frac{\left(1 + b/S_0^2 - \tau_c/2 + \nu\mathcal{K}_\varepsilon\right)}{2\left(1 - \tau_c/2 + \nu\mathcal{K}_\varepsilon\right)} - \mathcal{F}(\lambda)\,, \qquad \mathcal{F}(\lambda) \equiv \frac{\int_0^\infty w\left[(L_0-\lambda)^{-1}w^2\right]\rho\,d\rho}{\int_0^\infty w^2\rho\,d\rho}\,. \tag{3.37}$$

To determine whether (3.37) can have complex conjugate imaginary roots for some critical value of τ_c, we simply observe that (3.37) is identical in form to that in (3.28) for the Schnakenberg model if we replace α and $\mathcal{K}_0$ in (3.28) with b/S_0^2 and $\mathcal{K}_\varepsilon$. Therefore, the leading-order HB threshold occurs for the GS model occurs when $\tau \sim \tau_{c0} \equiv 2\left(1 - b/S_0^2\right)$. Since $\tau_{c0} > 0$ when $S_0 > S_{0c} \equiv \sqrt{b}$, we can use $\mathcal{K}_\varepsilon = \mathcal{K}_0 + \mathcal{O}(\nu\varepsilon^{\tau_{c0}})$ (see (3.18)) to approximate $\mathcal{K}_\varepsilon$ in (3.37) by $\mathcal{K}_0$ with an asymptotically negligible error. The asymptotic analysis to calculate a refined HB threshold and frequency is then exactly the same as for the Schnakenberg model and is summarized as follows.

Proposition 3.3. *Consider an N-spot quasi-equilibrium pattern for the GS model (1.3) in the regime where $D = D_0/\nu$ with $\nu \ll 1$ and along the upper branch of the bifurcation diagram in Figure 3, where $S_0 > \sqrt{b}$. Then, the modified NLEP (3.1a) with multiplier (3.34) has a Hopf bifurcation, corresponding to temporal oscillations in the spot amplitudes with the scaling law*

$$\tau_H \sim \frac{1}{\nu}\varepsilon^{-\tau_c}\,, \quad \tau_c = 2\left(1 - \frac{b}{S_0^2}\right) - \nu\log\nu + \tau_{c1}\nu + \tau_{c2}\nu^2 + \cdots\,; \quad \lambda \sim i\nu\left(\lambda_{I0} + \nu^2\lambda_{I2} + \cdots\right)\,. \tag{3.38}$$

Here $b \equiv \int_0^\infty \rho w^2\,d\rho \approx 4.935$, where $w(\rho)$ is the ground-state solution (1.4c), while the coeffi-

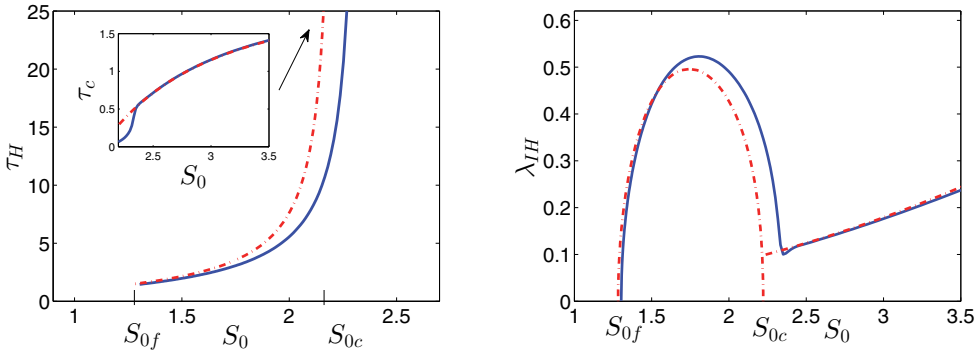

(a) τ_H versus S_0 (b) λ_{IH} versus S_0

Figure 7. *Left panel: HB threshold τ_H (solid curve) versus S_0 on the range $S_0 > S_{0f} = \sqrt{b/(1+\mu)}$ (see Figure 3) for a one-spot solution to the Gray–Scott model (1.2) centered at the origin of the unit disk with $\nu = 0.125$ and $\mu = 2$, as computed from (3.33) in which $\alpha = b/S_0^2$. The dot-dashed curve is the HB threshold for the conventional NLEP (2.24). In the insert, $\tau_c \equiv \nu \log(\tau_H \nu)$ from (3.33) is in close agreement with the asymptotic result in (3.38) on $S_0 > S_{0c} \equiv \sqrt{b}$. Right panel: λ_{IH} versus S_0 from (3.33) (solid curve), from the NLEP with a bilinear multiplier (2.24) (dot-dashed curve for $S_{0f} < S_0 < S_{0c}$), and from the asymptotic result (3.38) (dot-dashed curve for $S_0 > S_{0c}$).*

cients in (3.38) are given explicitly by

(3.39)
$$\tau_{c1} = 2\beta_k - \log \lambda_{I0}\,, \quad \tau_{c2} = \frac{\pi^2 S_0^2}{8b}(1 - 2\kappa_c)\,, \quad \lambda_{I0} = \frac{\pi S_0^2}{4b}\,, \quad \lambda_{I2} = \frac{\pi^3}{16}\left(\frac{S_0^2}{b}\right)^3 \left(\frac{1}{4} - \kappa_c\right)\,.$$

Here β_k and κ_c are defined in (3.35) and (2.7c), respectively.

The HB threshold and eigenvalue for a one-spot solution centered at the origin for the GS model (1.2) is plotted in Figure 7 when $\nu = 0.125$ and $\mu = 2$, for which $D_0 = 1$. For the GS model, this threshold is the root of (3.33), where $\theta_\lambda \equiv \sqrt{\nu\,(1 + i\tau\lambda_{IH})\,/D_0}$, and $\alpha = b/S_0^2$, where $S_0 > S_{0f} \equiv \sqrt{b/(1+\mu)}$ parametrizes the upper branch of the bifurcation diagram of Figure 3. In Figure 6 we compare these HB threshold values with that from the conventional NLEP theory (2.24), valid on $S_{0f} < S_0 < S_{0c} \equiv \sqrt{b}$, and with that from the asymptotic scaling law in (3.38), valid for $S_0 > S_{0c}$.

4. Refined HB thresholds for multispot patterns. The leading-order conventional NLEP analysis of section 2 for the parameter regime $D = D_0/\nu$ and $\tau = \mathcal{O}(1)$ showed that the HB threshold depends only on the number of spots and is independent of their spatial arrangement in the domain. This qualitative property of the HB threshold also occurs in the limit $\tau \gg 1$ for the modified NLEP analysis of section 3, which leads to the new scaling laws in Propositions 3.1–3.3. In this section, we numerically study the modified NLEPs of section 3 for the parameter range where the decay rate θ_λ in the reduced-wave Green's function (3.3) is $\mathcal{O}(1)$. It is in this transition regime where the HB threshold depends on the spot locations, and where there can be N distinct HB values corresponding to the distinct eigenvalues of the Green's matrix (3.4).

We will illustrate our theory for a quasi-equilibrium pattern where N spots are equally spaced on a ring of radius r_0, with $0 < r_0 < 1$, which is concentric within the unit disk, for which the spot centers are

$$\mathbf{x}_j = r_0 \left(\cos\left(\frac{2\pi j}{N}\right), \sin\left(\frac{2\pi j}{N}\right) \right)^T, \qquad j = 1, \ldots, N. \tag{4.1}$$

For r_0 we will take the steady-state ring radius determined in [11] from the leading-order-in-ν analysis for the $D = D_0/\nu \gg 1$ regime. In the unit disk, $G_\lambda(\mathbf{x};\xi)$ in (3.3) and its regular part are (see Appendix A.1 of [3])

$$G_\lambda(\mathbf{x};\xi) = \frac{1}{2\pi} K_0\left(\theta_\lambda |\mathbf{x}-\xi|\right) - \frac{1}{2\pi} \sum_{n=0}^{\infty} \sigma_n \cos\left(n(\psi-\psi_0)\right) \frac{K_n'(\theta_\lambda)}{I_n'(\theta_\lambda)} I_n\left(\theta_\lambda r\right) I_n\left(\theta_\lambda r_0\right), \tag{4.2a}$$

where $\sigma_0 \equiv 1$, $\sigma_n \equiv 2$ for $n \geq 1$, while $\mathbf{x} \equiv r(\cos\psi, \sin\psi)^T$, and $\xi \equiv r_0(\cos\psi_0, \sin\psi_0)^T$. The regular part is

$$R_\lambda = \frac{1}{2\pi}\left[\log\left(2\sqrt{D_0}\right) - \gamma - \frac{1}{2}\log\left(\nu(1+\tau\lambda)\right) \right] - \frac{1}{2\pi} \sum_{n=0}^{\infty} \sigma_n \frac{K_n'(\theta_\lambda)}{I_n'(\theta_\lambda)} \left[I_n\left(\theta_\lambda r_0\right) \right]^2, \tag{4.2b}$$

For a ring pattern, the symmetric Green's matrix $\mathcal{G}_\lambda$ in (3.4) also has a cyclic structure. This Green's matrix is obtained by a cyclic permutation of its first row $\boldsymbol{a}_\lambda \equiv (a_{\lambda,1}, \ldots, a_{\lambda,N})^T$, which is defined termwise by

$$a_{\lambda,1} \equiv R_\lambda; \qquad a_{\lambda,j} = G_{\lambda,j1} \equiv G_\lambda(\mathbf{x}_j;\mathbf{x}_1), \quad j = 2, \ldots, N. \tag{4.3}$$

The matrix spectrum $\mathcal{G}_\lambda \mathbf{v}_j = \kappa_{\lambda,j}\mathbf{v}_j$ is readily calculated as in section 6 of [8]. The synchronous eigenpair of $\mathcal{G}_\lambda$ is

$$\kappa_{\lambda,1} = \sum_{n=1}^{N} a_{\lambda,n}, \qquad \mathbf{v}_1 = (1, \ldots, 1)^T, \tag{4.4a}$$

while the other eigenvalues, corresponding to the asynchronous modes for which $\mathbf{v}_j^T \mathbf{v}_1 = 0$ for $j = 2, \ldots, N$, are

$$\kappa_{\lambda,j} = \sum_{n=0}^{N-1} \cos\left(\frac{2\pi(j-1)\,n}{N}\right) a_{\lambda,n+1}, \qquad j = 2, \ldots, N. \tag{4.4b}$$

Since $\kappa_{\lambda,j} = \kappa_{\lambda,N+2-j}$ for $j = 2, \ldots, \lceil N/2 \rceil$, there are $\lceil N/2 \rceil - 1$ pairs of degenerate eigenvalues for $\mathcal{G}_\lambda$. Here the ceiling function $\lceil x \rceil$ is defined as the smallest integer not less than x. When N is even, there is an eigenvalue of multiplicity one given by $\kappa_{\lambda,\frac{N}{2}+1} = \sum_{n=0}^{N-1} (-1)^n a_{n+1}$. The other eigenvectors for $j = 2, \ldots, \lceil N/2 \rceil$ are

$$\begin{aligned} \mathbf{v}_j &= \left(1, \cos\left(\frac{2\pi(j-1)}{N}\right), \ldots, \cos\left(\frac{2\pi(j-1)(N-1)}{N}\right)\right)^T, \\ \mathbf{v}_{N+2-j} &= \left(0, \sin\left(\frac{2\pi(j-1)}{N}\right), \ldots, \sin\left(\frac{2\pi(j-1)(N-1)}{N}\right)\right)^T. \end{aligned} \tag{4.4c}$$

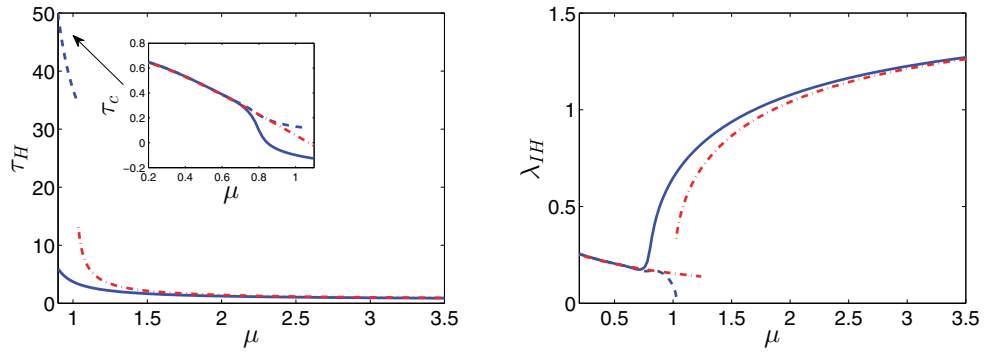

(a) τ_H versus μ (b) λ_{IH} versus μ

Figure 8. *HB threshold τ_H (left panel) and eigenvalue λ_{IH} (right panel) versus μ for a two-spot ring pattern in the unit disk for the GM model (1.1) when $r_0 = 0.452$ and $\nu = 0.1$. The solid curves in the left and right panel are for the synchronous mode $j = 1$ mode, while the dotted curves are for the asynchronous $j = 2$ mode, both computed from (4.5). The dot-dashed curves for $\mu > 1$ are from the conventional NLEP theory (2.13), while the dot-dashed curves for $\mu < 1$ are from the asymptotic scaling law (3.19). In the insert in the left panel we plot $\tau_c \equiv \nu \log(\tau_H \nu)$. The HB thresholds for the synchronous and asynchronous modes are clearly distinct on $0.8 < \mu < 1$, with the synchronous mode yielding the smaller of the two values for τ_H. The HB eigenvalue for the asynchronous mode vanishes just beyond $\mu = 1$.*

Finally, when N is even, there is an additional eigenvector given by $\mathbf{v}_{\frac{N}{2}+1} = (1, -1, \ldots, -1)^T$. By using the explicit formulae for G_λ and its regular part from (4.2), the eigenvalues $\kappa_{\lambda,j}$ of the Green's matrix $\mathcal{G}_\lambda$ are then easily computed from (4.4a) and (4.4b).

To determine the HB thresholds for the GM model (1.1) from the modified NLEP (3.1), we must numerically determine the roots of

(4.5)
$$\mathrm{Re}(\kappa_{\lambda,j}) = -\frac{1}{2\pi\nu}\left(1 - \frac{(1+\mu)\mathcal{F}_R}{2\left(\mathcal{F}_R^2 + \mathcal{F}_I^2\right)}\right), \qquad \mathrm{Im}(\kappa_{\lambda,j}) = -\frac{1}{4\pi\nu}\frac{(1+\mu)\mathcal{F}_I}{\left(\mathcal{F}_R^2 + \mathcal{F}_I^2\right)}, \qquad j = 1, \ldots, N,$$

where $\mathcal{F}_R(\lambda_I)$ and $\mathcal{F}_I(\lambda_I)$ are defined in (2.6). For a two-spot ring pattern with $r_0 = 0.452$ and $\nu = 0.1$, in Figure 8 we plot the HB threshold values τ_H and λ_{IH} versus μ for $j = 1$ (synchronous, solid curves) and for $j = 2$ (asynchronous, dotted curves), as computed from (4.5). Results from the conventional NLEP theory for $\mu > 1$ (2.13) and from the asymptotic scaling law for $\mu < 1$ (3.19) are indicated by the dot-dashed curves. We observe that on the range $\mu < 1$, the HB thresholds for τ_H and λ_{IH} for the synchronous and asynchronous modes essentially coincide only up to around $\mu = 0.8$. On the range $0.8 < \mu < 1$, the HB thresholds for the two modes are distinct, with the synchronous mode yielding the smaller τ_H. From the right panel of Figure 8, the HB eigenvalue for the asynchronous mode is positive for $\mu < 1$, but vanishes at some critical value of μ that is slightly above $\mu = 1$. This is consistent with conventional NLEP theory, in that it was shown in section 2.1 for the regime $\tau = \mathcal{O}(1)$ and $D = D_0/\nu$ that the asynchronous mode does not undergo a Hopf bifurcation when $\mu > 1$, but is unstable due to a positive real eigenvalue. This mechanism whereby the purely imaginary pair of complex conjugate eigenvalues associated with the asynchronous mode collides at the

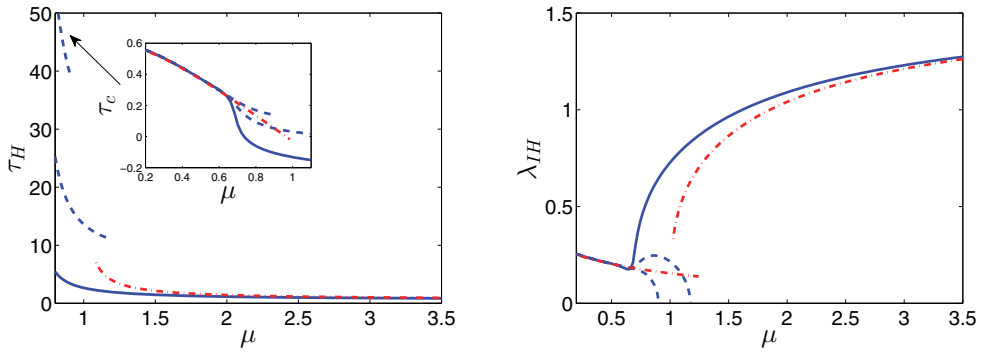

(a) τ_H versus μ (b) λ_{IH} versus μ

Figure 9. *HB thresholds for the GM model (1.1) for a five-spot ring pattern with $r_0 = 0.6252$ and $\nu = 0.1$. For $N = 5$, there is an HB for the synchronous mode $j = 1$ (solid curves) and for two distinct asynchronous modes $j = 2, 3$ (dotted curves), as obtained numerically from (4.5). The dot-dashed curves for $\mu > 1$ are from the conventional NLEP theory (2.13), while the dot-dashed curves for $\mu < 1$ are from the asymptotic scaling law (3.19), where we plot $\tau_c \equiv \nu \log(\tau_H \nu)$. The HB threshold value of τ is smallest for the synchronous mode. For each of the two asynchronous modes, the HB thresholds exist on $\mu > 0$ only up to some critical value near $\mu = 1$, where the Hopf eigenvalue vanishes.*

origin $\lambda = 0$ of the spectral plane at some critical value μ_c of μ and produces a positive real eigenvalue when $\mu > \mu_c$ is similar to that found in the study of the stabiliy of GM spike patterns in one dimension (see Figure 18 of [25]).

A very similar scenario occurs for larger N. In particular, in Figure 9 we plot the HB threshold values, as computed from (4.5), for a five-spot pattern with $\nu = 0.1$ and ring radius $r_0 = 0.6252$. For $N = 5$, we have $\kappa_{\lambda,i} = \kappa_{\lambda,7-i}$ for $i = 2, 3$, and so there are exactly two distinct asynchronous modes. From the insert in the left panel of Figure 9, and from the right panel of Figure 9, we conclude that the HB values of τ_H and λ_{IH} for the synchronous and asynchronous modes essentially coincide on $\mu < 0.65$, where they are well-approximated by the scaling law (3.19). In addition, the conventional NLEP theory (2.13) provides a decent approximation to the HB threshold for the synchronous mode when $\mu > 1$. Finally, the HB eigenvalue for each of the two asynchronous modes vanishes at some critical value of μ near $\mu = 1$.

A qualitatively similar behavior of the HB threshold occurs for a ring-pattern of spots for the GS model (1.2) and the Schnakenberg model (1.3). For illustration, we will only consider the latter model here. For the Schnakenberg model, any HB value for the modified NLEP (3.1a) with multiplier (3.24) is a root of

$$\text{Re}(\kappa_{\lambda,j}) = -\frac{1}{2\pi\nu}\left(1 + \frac{\alpha\,(1-2\mathcal{F}_R)}{(1-2\mathcal{F}_R)^2 + 4\mathcal{F}_I^2}\right), \quad \text{Im}(\kappa_{\lambda,j}) = -\frac{1}{\pi\nu}\frac{\alpha\mathcal{F}_I}{\left[(1-2\mathcal{F}_R)^2 + 4\mathcal{F}_I^2\right]}, \quad j = 1, \ldots, N\,. \tag{4.6}$$

For the unit disk, $\mu = 2\pi N D_0/|\Omega| = 2ND_0$ and α is related to the feed-rate parameter $\mathcal{A}$ in (1.3) (see (3.24)) by $\alpha = 4bD_0N^2\mathcal{A}^{-2}$, where $b \equiv \int_0^\infty \rho w^2\,d\rho \approx 4.935$.

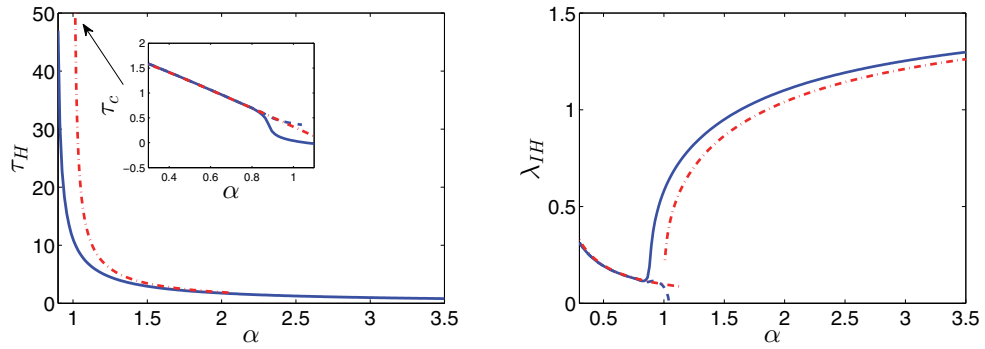

(a) τ_H versus α (b) λ_{IH} versus α

Figure 10. *HB threshold τ_H (left panel) and eigenvalue λ_{IH} (right panel) versus α for a two-spot ring pattern in the unit disk for the Schnakenberg model (1.3) when $r_0 = 0.452$, $\nu = 0.125$, and $\mu = 4$, so that $D_0 = 1$. The solid and dotted curves, computed from (4.6), are for the synchronous ($j = 1$) and asynchronous ($j = 2$) modes, respectively. The dot-dashed curves for $\alpha > 1$ and for $\alpha < 1$ are from the conventional NLEP theory (2.18) and the new scaling law (3.31), respectively. From the left panel, the HB eigenvalue for the asynchronous mode vanishes just beyond $\alpha = 1$.*

In Figure 10 we plot the HB threshold values versus α, as computed from (4.6), for a two-spot pattern with $\nu = 0.125$, ring radius $r_0 = 0.452$, and with $\mu = 4$, so that $D_0 = 1$. We observe that the HB values of τ_H and λ_{IH} for the synchronous and asynchronous modes essentially coincide on $\alpha < 0.85$, where they are well-approximated by the new scaling law (3.31). Moreover, the conventional NLEP theory, given by the parameterization (2.18), approximates well the HB threshold for the synchronous mode when $\alpha > 1$. We observe that the HB eigenvalue for the asynchronous mode vanishes at some critical value of α slightly above $\alpha = 1$.

Finally, in Figure 11 we plot the HB threshold values versus α for a five-spot ring pattern with $\nu = 0.125$, ring radius $r_0 = 0.6252$, and with $\mu = 10$, so that we maintain $D_0 = 1$. The results are qualitatively identical to that discussed in the caption of Figure 9 for a five-spot pattern for the GM model.

5. HB thresholds for moderately small ν: Numerical validation. In this section we show how to accurately determine the HB threshold for a ring pattern of spots for the Schnakenberg model (1.3) when $\nu = -1/\log\varepsilon$ is only moderately small. In contrast to NLEP theory, which is a leading-order-in-ν theory, the resulting problem formulated below for the HB threshold effectively incorporates all terms in powers of ν. The formulation of this problem relies on some results in Appendix A.

For a quasi-equilibrium ring pattern of N spots, and with $D = D_0/\nu$, the common spot source strength is $S_j = S_c = \mathcal{A}\sqrt{\nu}/(2\pi N\sqrt{D_0})$ for $j = 1, \ldots, N$. From (A.1), the common core problem near each spot is

$$\Delta_\rho \mathcal{V}_c - \mathcal{V}_c + \mathcal{U}_c\mathcal{V}_c^2 = 0\,, \qquad \mathcal{V}_c'(0) = 0\,, \quad \mathcal{V}_c \to 0 \quad \text{as} \quad \rho \to \infty\,, \tag{5.1a}$$

$$\Delta_\rho \mathcal{U}_c = \mathcal{U}_c\mathcal{V}_c^2\,, \qquad \mathcal{U}_c'(0) = 0\,, \quad \mathcal{U}_c \sim S_c\log\rho + \mathcal{D}(S_c)\,, \quad \text{as} \quad \rho \to \infty\,. \tag{5.1b}$$

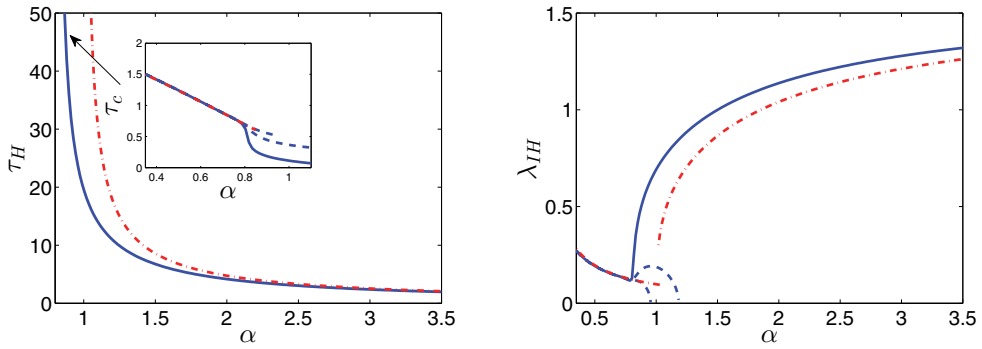

(a) τ_H versus α (b) λ_{IH} versus α

Figure 11. *HB threshold τ_H (left panel) and eigenvalue λ_{IH} (right panel) versus α for a five-spot ring pattern in the unit disk for the Schnakenberg model (1.3) when $r_0 = 0.6252$, $\nu = 0.125$, and $\mu = 10$, so that $D_0 = 1$. The solid and dotted curves, computed from (4.6), are for the synchronous ($j = 1$) and asynchronous ($j = 2, 3$) modes, respectively. The dot-dashed curves for $\alpha > 1$ and for $\alpha < 1$ are from the conventional NLEP theory (2.18) and the new scaling law (3.31), respectively. From the left panel, the HB eigenvalue for each of the two asynchronous modes vanishes near $\alpha = 1$.*

Upon linearizing around this particular quasi-equilibrium solution, we use (A.16) and (A.10) to obtain the following spectral problem

$$(I(1 + \nu B_c) + 2\pi\nu\mathcal{G}_\lambda)\,\mathbf{C} = \mathbf{0}\,, \tag{5.2}$$

where $\mathbf{C} \equiv (C_1, \ldots, C_N)^T$ and $B_c = B_c(\lambda, S_c)$ is obtained from the BVP system

$$\Delta_\rho \Phi_c - \Phi_c + 2\mathcal{U}_c\mathcal{V}_c\Phi_c + \mathcal{V}_c^2 N_c = \lambda\Phi_c\,, \qquad \Phi_c'(0) = 0\,, \quad \Phi_c \to 0 \quad \text{as} \quad \rho \to \infty\,, \tag{5.3a}$$

$$\Delta_\rho N_c - \mathcal{V}_c^2 N_c = 2\mathcal{U}_c\mathcal{V}_c\Phi_c\,, \qquad N_c'(0) = 0\,, \quad N_c \sim \log\rho + B_c\,. \quad \text{as} \quad \rho \to \infty\,, \tag{5.3b}$$

In (5.2), $\mathcal{G}_\lambda$ is the eigenvalue-dependent Green's matrix defined in (3.4) in terms of the Green's function of (3.25). For this N-spot ring pattern, the matrix spectrum of $\mathcal{G}_\lambda$ is as given in (4.3)–(4.4c).

In this way, we obtain from (5.2) that the discrete eigenvalues λ characterizing the linear stability of a ring pattern of spots are the union of the roots of

$$\kappa_{\lambda,j} = -\frac{1}{2\pi\nu}\,(1 + \nu B_c)\,, \qquad j = 1\,, \ldots, N\,, \tag{5.4}$$

where $\kappa_{\lambda,j}$ is given explicitly in terms of the first row of the Green's matrix by (4.4b). In (5.4), $B_c = B_c(\lambda, S_c)$ is to be computed numerically from (5.3) in terms of the numerical solution to the core problem (5.1). To determine the HB threshold for the $j = 1$ synchronous mode, and for the remaining asynchronous modes with $j > 1$, we set $\lambda = i\lambda_I$ in (5.4) and use Newton's method on the complex-valued equation (5.4) to compute the HB values τ_H and λ_{IH} for each $j = 1, \ldots, N$.

To illustrate the theory, we let $N = 4$ and take $r_0 = 0.5986$, which is the steady-state ring radius when $N = 4$ (cf. [11]). For $\varepsilon = 0.01$ and $D = D_0/\nu$ with $D_0 = 1$, in Figure 12

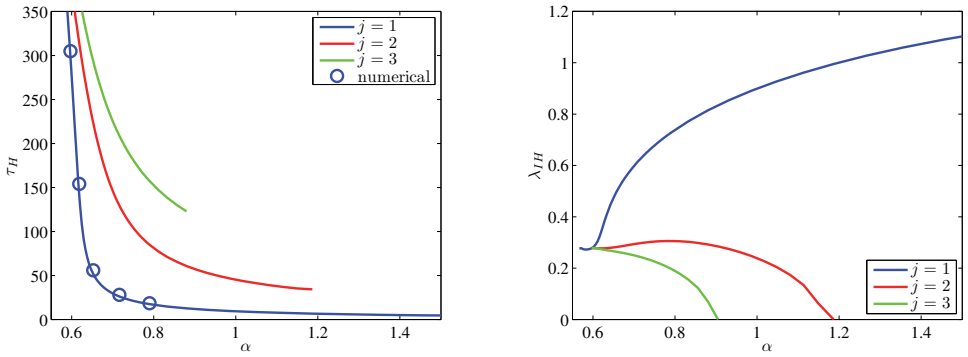

(a) τ_H versus α (b) λ_{IH} versus α

Figure 12. *HB threshold τ_H (left panel) and eigenvalue λ_{IH} (right panel) versus α for a four-spot ring pattern in the unit disk for the Schnakenberg model (1.3) when $r_0 = 0.5986$, $\varepsilon = 0.01$, and $D = D_0/\nu$, where $D_0 = 1$ and $\nu = -1/\log\varepsilon$. The solid curves were computed from the full asymptotic theory (5.4), which is accurate to all orders in ν. The $j = 1$ mode is the synchronous mode, while the $j = 2$ and $j = 3$ modes correspond to asynchronous oscillations. The $j = 4$ curve is identical to that for $j = 2$. Left panel: as τ increases, the synchronous mode is the first to go unstable. The $j = 3$ curve ends at $\alpha \approx 0.905$. For $\alpha > 0.905$, there is a real positive eigenvalue for any value of τ, corresponding to a competition instability. The open circles correspond to thresholds obtained from determining the HB threshold from full numerical solutions of the Schnakenberg PDE (1.3). Right panel: the HB eigenvalue λ_{IH}. As α approaches the competition threshold, the eigenvalue for the $j = 3$ mode approaches the origin along the imaginary axis.*

we plot the HB values, computed from (5.4), as a function of α where $\alpha \equiv 4bD_0N^2\mathcal{A}^{-2}$ with $b \approx 4.935$. From Figure 12(a) we observe that the HB value of τ for the synchronous mode $j = 1$ is the smallest, and so it is this mode which sets the HB threshold. The two distinct asynchronous modes have larger HB values for τ and, as expected, the thresholds for each of these modes exist only when α is less than some critical value near $\alpha = 1$. From Figure 12(b), we observe that the corresponding Hopf frequency vanishes at these critical values of α.

Finally, we compare our asymptotic theory with results from full PDE numerical simulations of the Schnakenberg model (1.3) computed using the adaptive finite element solver FlexPDE6 [7] for the specific four-spot pattern of Figure 12 with $\mathcal{A} = 22.8$. For this value of $\mathcal{A}$, we have $\alpha \approx 0.6184$, and Figure 12(a) for the $j = 1$ mode yields the asymptotic prediction $\tau_H \approx 153$. For the parameter value $\tau = 158$, which slightly exceeds the HB prediction $\tau_H \approx 153$, in Figure 13 we show that a random initial perturbation of the spot amplitudes will eventually lead to synchronized spot amplitude oscillations as time increases. Since the range of these oscillations is small, the full numerical results in Figure 14 over a much longer time interval than in Figure 13(b) suggest that the Hopf bifurcation for this parameter set is supercritical.

6. Discussion. We have provided a detailed analysis of the parameter values for the onset of temporal oscillations of the spot amplitudes for multispot patterns associated with three singularly perturbed two-component RD systems in a bounded 2-D domain. In these systems, the two bifurcation parameters are the reaction-time parameter τ and the inhibitor diffusivity D. In the limit of large diffusivity $D = D_0/\nu \gg 1$ with $D_0 = \mathcal{O}(1)$, the linear stability

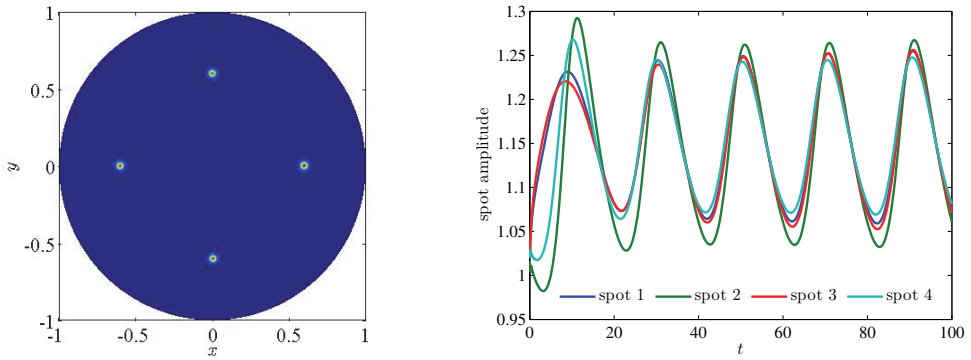

(a) four-spot ring pattern at steady-state (b) spot amplitudes versus t

Figure 13. *Full numerical computations in the unit disk for the Schnakenberg model* (1.3) *using FlexPDE*6 [7] *showing synchronous oscillations in the spot amplitudes for a four-spot ring pattern with ring radius* $r_0 = 0.5986$ *and with parameters* $\varepsilon = 0.01$, $A = 22.8$, $\tau = 158$, *and* $D = D_0/\nu$, *where* $D_0 = 1$ *and* $\nu = -1/\log\varepsilon$. *This corresponds to* $\alpha = 0.6184$ *in Figure* 12. *Left panel: when* $r_0 = 0.5986$, *the four-spot ring pattern is at a steady-state configuration. Right panel: growing temporal oscillations of the amplitudes of the four spots when* $\tau = 158$ *is set slightly above the HB threshold* $\tau_H \approx 153$, *as predicted by the asymptotic theory* (5.4). *The HB thresholds for the asynchronous modes are* $\tau_{H2} \approx 312$ *and* $\tau_{H3} \approx 367$. *The steady-state was perturbed by a small random perturbation. However, the oscillations quickly synchronize as predicted by the asymptotic theory, with the amplitudes of the four spots exhibiting in-phase oscillations of increasing amplitude. (The labels of the spots are as in the caption of Figure* 14.*) The angular frequency of the oscillations is approximately* 0.31, *close to the predicted value of* $\lambda_{IH} = 0.334$ *from* (5.4).

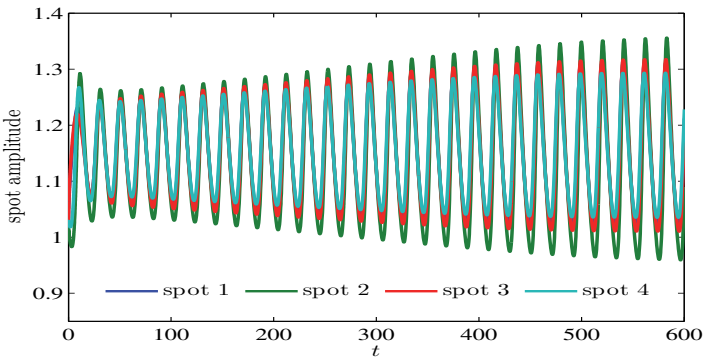

Figure 14. *Plot of the spot amplitudes for the four-spot ring pattern of Figure* 13 *over a larger time interval, as computed from full PDE simulations of* (1.3). *The occurrence of small amplitude temporal oscillations suggests that the Hopf bifurcation for this parameter set is supercritical. The labels of the four spots are spot* 1, *positive* x*-axis; spot* 2, *positive* y*-axis; spot* 3, *negative* x*-axis; spot* 4, *negative* y*-axis.*

properties of multispot patterns on $\mathcal{O}(1)$ time-scales is determined by the spectra of an NLEP. For the conventional regime where $\tau = \mathcal{O}(1)$, considered originally in [27], [28], [29], [30], [31], our new parameterization of the NLEP has shown that synchronous temporal oscillations in the spot amplitudes due to a Hopf bifurcation can only occur on the range $D_0 > D_{0c}$, where

$D_{0c} > 0$ is the competition stability threshold. For $D_0 < D_{0c}$ no spot amplitude oscillations occur for any $\tau = \mathcal{O}(1)$. To analyze whether a Hopf bifurcation can occur when $\tau \gg 1$ and $D_0 < D_{0c}$ we derive a new modified NLEP appropriate to this regime by considering a new distinguished limit of the reduced-wave Green's function. From an analysis of this modified NLEP we have shown for the range $D_0 < D_{0c}$ that a Hopf bifurcation will occur at some threshold $\tau = \tau_H \gg 1$, where $\tau_H \sim \nu^{-1}\varepsilon^{-\tau_c} \gg 1$ for some τ_c satisfying $0 < \tau_c < 2$. The exponent τ_c in this anomalous scaling law was calculated for each of the three RD systems. This exponent is independent of the configuration of spots in the domain. Our detailed analysis of the Hopf bifurcation threshold resolves a long-standing open problem in NLEP theory (cf. [33]).

The anomalous scaling law for the Hopf bifurcation threshold τ_H when $D < D_{0c}/\nu$ is not uniformly valid as D tends to the competition threshold D_{0c}/ν from below. When D is near this competition threshold, in section 4 it was shown that the Hopf bifurcation threshold depends on the spatial configuration of spots in the domain. In section 4 this Hopf threshold was computed numerically from the modified NLEP only for a ring pattern of spots inside the unit disk, where both the Green's matrix and its spectra are readily available. It would be worthwhile to extend this methodology to compute the Hopf threshold for an arbitrary spatial configuration of spots in a general 2-D domain when D is near the competition threshold. For an arbitrary 2-D domain this extension would require computing the Green's function using fast multipole numerical methods of [13] and determining the matrix spectra of the Green's matrix numerically.

Finally, now that the conditions for the onset of Hopf bifurcations of multispot patterns in two dimensions are better understood for the regime $D = D_0/\nu$, it would be worthwhile to develop a weakly nonlinear theory to characterize whether spot amplitude oscillations are subcritical or supercritical. For the parameter values of Figure 14 used for the Schnakenberg model, the Hopf bifurcation is most likely supercritical. Although such a weakly nonlinear theory has been recently developed in [22] for 1-D spike patterns, the extension of this theory to treat 2-D spot patterns will be challenging.

Appendix A. The Schnakenberg model. We first use the method of matched asymptotic expansions, as in [11], to construct an N-spot quasi-equilibrium solution to the Schnakenberg model (1.3), where the spots are centered at $\mathbf{x}_j \in \Omega$ for $j = 1, \dots, N$.

In the inner region near $\mathbf{x} = \mathbf{x}_j$ we introduce the inner variable $\mathbf{y} = \varepsilon^{-1}(\mathbf{x} - \mathbf{x}_j)$ with $\rho = |\mathbf{y}|$ and look for a locally radially symmetric solution in the form $v = \sqrt{D}\,\mathcal{V}_j(\rho) + \cdots$ and $u = (\mathcal{A}\sqrt{D})^{-1}\mathcal{U}_j(\rho) + \cdots$. By substituting this expansion into the steady-state equations of (1.3), we get that $\mathcal{V}_j$ and $\mathcal{U}_j$ are solutions to the following core problem, defined on $\rho > 0$, which is parameterized by the unknown source strength $S_j > 0$:

$$\Delta_\rho \mathcal{V}_j - \mathcal{V}_j + \mathcal{U}_j \mathcal{V}_j^2 = 0\,, \qquad \mathcal{V}_j'(0) = 0\,, \quad \mathcal{V}_j \to 0\,, \quad \text{as} \quad \rho \to \infty\,, \tag{A.1a}$$

$$\Delta_\rho \mathcal{U}_j = \mathcal{U}_j \mathcal{V}_j^2\,, \qquad \mathcal{U}_j'(0) = 0\,, \quad \mathcal{U}_j \sim S_j \log\rho + \mathcal{D}(S_j)\,, \quad \text{as} \quad \rho \to \infty\,. \tag{A.1b}$$

Here $\Delta_\rho \equiv \partial_{\rho\rho} + \rho^{-1}\partial_\rho$. The function $\mathcal{D}(S_j)$ was computed numerically in section 2.1 of [11].

The source strengths S_j for $j = 1, \dots, N$ are determined by matching the solution to the core problem (A.1) near each $\mathbf{x}_j$ to an outer solution for u. This outer problem is

$$\Delta u = -1 + \frac{2\pi\sqrt{D}}{\mathcal{A}} \sum_{i=1}^{N} S_i \, \delta(\mathbf{x} - \mathbf{x}_i) \,, \quad \mathbf{x} \in \Omega \,; \qquad \partial_n u = 0 \,, \quad \mathbf{x} \in \partial\Omega \,, \tag{A.2a}$$

$$u \sim \frac{1}{\mathcal{A}\sqrt{D}} \left[S_j \log |\mathbf{x} - \mathbf{x}_j| + \mathcal{D}(S_j) + \frac{S_j}{\nu} \right] , \quad \text{as} \quad \mathbf{x} \to \mathbf{x}_j \,, \quad j = 1, \dots, N \,, \tag{A.2b}$$

where $\nu \equiv -1/\log\varepsilon$. The solution to (A.2) is

$$u(\mathbf{x}) = -\frac{2\pi}{\mathcal{A}\sqrt{D}} \left(\sum_{i=1}^{N} S_i G_0(\mathbf{x}; \mathbf{x}_i) + \bar{u} \right) , \qquad \text{provided that} \qquad \sum_{i=1}^{N} S_i = \frac{\mathcal{A}|\Omega|}{2\pi\sqrt{D}} \,. \tag{A.3}$$

Here $\bar{u}$ is a constant to be found and $G_0(\mathbf{x}; \mathbf{x}_i)$ is the Neumann Green's function, which satisfies

$$\Delta G_0 = \frac{1}{|\Omega|} - \delta(\mathbf{x} - \mathbf{x}_i) \,, \quad \mathbf{x} \in \Omega \,; \qquad \partial_n G_0 = 0 \,, \quad \mathbf{x} \in \partial\Omega \,, \tag{A.4a}$$

$$G_0(\mathbf{x}; \mathbf{x}_i) = -\frac{1}{2\pi} \log |\mathbf{x} - \mathbf{x}_i| + R_0(\mathbf{x}_i) + o(1) \,, \quad \text{as} \quad \mathbf{x} \to \mathbf{x}_i \,; \qquad \int_\Omega G_0 \, d\mathbf{x} = 0 \,. \tag{A.4b}$$

By matching the local behavior of u as $\mathbf{x} \to \mathbf{x}_j$ with the far-field of $\mathcal{U}_j$ as $\rho \to \infty$, we derive that S_j for $j = 1, \dots, N$ and $\bar{u}$ satisfy the $N+1$ dimensional nonlinear algebraic system

$$S_j + 2\pi\nu \left(S_j R_{0,j} + \sum_{i \neq j}^{N} S_i G_{0,ji} \right) + \nu \mathcal{D}(S_j) = -2\pi\nu\bar{u} \,, \quad j = 1 \,, \dots, N \,; \qquad \sum_{i=1}^{N} S_i = \frac{\mathcal{A}|\Omega|}{2\pi\sqrt{D}} \,, \tag{A.5}$$

where $G_{0,ji} \equiv G_0(\mathbf{x}_j; \mathbf{x}_i)$ and $R_{0,j} \equiv R_0(\mathbf{x}_j)$.

When $D = D_0/\nu \gg 1$, the last expression in (A.5) yields that $S_j = \mathcal{O}(\sqrt{\nu}) \ll 1$. For $S_j \ll 1$ it was shown in Appendix A of [9] that

$$\mathcal{U}_j \sim \frac{b}{S_j} + \cdots \,, \qquad \mathcal{V}_j \sim \frac{S_j w}{b} + \cdots \,, \qquad \mathcal{D}(S_j) \sim \frac{b}{S_j} \tag{A.6}$$

for $S_j \ll 1$, where $b \equiv \int_0^\infty \rho w^2 \, d\rho \approx 4.935$, and $w(\rho)$ is the ground-state solution of (1.4c). We then use the dominant balance $S_j = \sqrt{\nu}\tilde{S}_j$ to reduce (A.5) to leading-order in ν to

$$\tilde{S}_j + \frac{b}{\tilde{S}_j} = -2\pi\sqrt{\nu}\bar{u} \,, \qquad \sum_{i=1}^{N} \tilde{S}_i = \frac{\mathcal{A}|\Omega|}{2\pi\sqrt{D_0}} \,. \tag{A.7}$$

We consider only *symmetric* quasi-equilibrium N-spot solutions (cf. [31]), where there is a common leading-order source strength. From (A.7) the common source strength is $\tilde{S}_j = S_0 \equiv \mathcal{A}|\Omega|/(2\pi N\sqrt{D_0})$.

Next, we examine whether the N-spot quasi-equilibrium solution, denoted by v_e and u_e, can become unstable on an $\mathcal{O}(1)$ time-scale due to instabilities in the spot amplitudes. To do so, we introduce the perturbation $u = u_e + e^{\lambda t}\eta$ and $v = v_e + e^{\lambda t}\phi$ to obtain, from (1.3), the following eigenvalue problem with $\partial_n\phi = \partial_n\eta = 0$ on $\partial\Omega$:

$$\varepsilon^2\Delta\phi - \phi + 2\mathcal{A}u_e v_e\phi + \mathcal{A}v_e^2\eta = \lambda\phi\,, \qquad D\Delta\eta - \tau\lambda\eta = \varepsilon^{-2}\left(2u_e v_e\phi + v_e^2\eta\right)\,, \qquad \mathbf{x}\in\Omega\,. \tag{A.8}$$

In the inner region near the jth spot we look for a leading-order locally radially symmetric solution as

$$\phi = \sqrt{D}\Phi_j(\rho) + \cdots\,, \qquad \eta = \frac{1}{\mathcal{A}\sqrt{D}}N_j(\rho) + \cdots\,, \tag{A.9}$$

where $\mathbf{y} = \varepsilon^{-1}(\mathbf{x} - \mathbf{x}_j)$ and $\rho = |\mathbf{y}|$. Upon substituting (A.9) into (A.8), and using $u_e v_e \sim \mathcal{A}^{-1}\mathcal{U}_j\mathcal{V}_j$ and $v_e^2 \sim D\mathcal{V}_j^2$, we obtain, on $\rho > 0$, that Φ_j and N_j satisfy

$$\Delta_\rho\Phi_j - \Phi_j + 2\mathcal{U}_j\mathcal{V}_j\Phi_j + \mathcal{V}_j^2 N_j = \lambda\Phi_j\,, \qquad \Phi_j'(0) = 0\,, \quad \Phi_j \to 0 \quad \text{as} \quad \rho\to\infty\,, \tag{A.10a}$$

$$\Delta_\rho N_j - \mathcal{V}_j^2 N_j = 2\mathcal{U}_j\mathcal{V}_j\Phi_j\,, \qquad N_j'(0) = 0\,, \quad N_j \sim C_j\log\rho + B_j\,, \quad \text{as} \quad \rho\to\infty\,, \tag{A.10b}$$

provided that τ is sufficiently small so that

$$\frac{\varepsilon^2\tau\lambda}{D} \ll 1\,. \tag{A.11}$$

In (A.10), $B_j = B_j(\lambda, S_j)$ must, in general, be computed numerically. Since (A.10) is a homogeneous linear system, we can, in principle, write $B_j = C_j\tilde{B}_j(\lambda, S_j)$. We will show below that the unknown coefficients C_j for $j = 1,\ldots,N$ are obtained from the eigenvectors of a matrix eigenvalue problem. Since Φ_j is proportional to C_j, we can interpret the coefficients as perturbations to the amplitudes of the spots, owing to the fact that the globally defined activator concentration v for a perturbed N-spot quasi-equilibrium solution has the form

$$v \sim \sum_{j=1}^{N}\sqrt{D}\left(\mathcal{V}_j\left[\varepsilon^{-1}|\mathbf{x}-\mathbf{x}_j|\right] + e^{\lambda t}\Phi_j\left[\varepsilon^{-1}|\mathbf{x}-\mathbf{x}_j|\right]\right)\,. \tag{A.12}$$

To derive a matrix eigenvalue problem for $C_1,\ldots,C_N$, we must match the inner solution N_j to an outer solution for η. The outer problem for η is simply

$$\Delta\eta - \frac{\tau\lambda}{D}\eta = \frac{2\pi}{\mathcal{A}\sqrt{D}}\sum_{i=1}^{N}C_i\,\delta(\mathbf{x}-\mathbf{x}_i)\,, \quad \mathbf{x}\in\Omega\,; \qquad \partial_n\eta = 0\,, \quad \mathbf{x}\in\partial\Omega\,, \tag{A.13a}$$

$$\eta \sim \frac{C_j}{\mathcal{A}\sqrt{D}}\left[\log|\mathbf{x}-\mathbf{x}_j| + B_j + \frac{1}{\nu}\right], \quad \text{as} \quad \mathbf{x}\to\mathbf{x}_j\,, \quad j = 1,\ldots,N\,. \tag{A.13b}$$

The solution to (A.13) is

$$\eta = -\frac{2\pi}{\mathcal{A}\sqrt{D}}\sum_{i=1}^{N}C_i G_\lambda(\mathbf{x};\mathbf{x}_i)\,, \tag{A.14}$$

where $G_\lambda(\mathbf{x};\mathbf{x}_i)$ is the Green's function satisfying (3.25). By asymptotically matching the local behavior of η as $\mathbf{x}\to\mathbf{x}_j$ to the far-field behavior of the inner solution $\eta=(\mathcal{A}\sqrt{D})^{-1}N_j$, we readily derive the matrix problem

$$C_j+2\pi\nu\left(R_{\lambda,j}C_j+\sum_{i\neq j}^{N}C_iG_{\lambda,ji}\right)+\nu B_j=0\,,\qquad j=1\,,\ldots,N\,. \tag{A.15}$$

Here $G_{\lambda,ji}\equiv G_\lambda(\mathbf{x}_j;\mathbf{x}_i)$, while $R_{\lambda,j}\equiv R_\lambda(\mathbf{x}_j)$ is the regular part of G_λ at $\mathbf{x}=\mathbf{x}_j$ (see (3.25)). In matrix form, (A.15) is

$$(I+2\pi\nu\mathcal{G}_\lambda)\,\mathbf{C}+\nu\mathbf{B}=\mathbf{0}\,, \tag{A.16}$$

where $\mathbf{C}\equiv(C_1,\ldots,C_N)^T$, $\mathbf{B}\equiv(B_1,\ldots,B_N)^T$, and $\mathcal{G}_\lambda$ is the $N\times N$ symmetric Green's matrix given in (3.4) in terms of the Green's function of (3.25).

For the parameter range where $D=D_0/\nu\gg 1$ with $\nu\ll 1$, we now derive an NLEP from (A.10) and (A.16) for the case where there is a common spot source strength $S_j=\sqrt{\nu}S_0$ with $S_0\equiv\mathcal{A}|\Omega|/(2\pi N\sqrt{D_0})$. In this parameter range, we use (A.6) to obtain $\mathcal{U}_j\sim b/[\sqrt{\nu}S_0]$ and $\mathcal{V}_j\sim\sqrt{\nu}S_0w/b$, so that (A.10) reduces, when written in matrix form, to

$$L_0\mathbf{\Phi}+\frac{\nu S_0^2w^2}{b^2}\mathbf{N}=\lambda\mathbf{\Phi}\,,\qquad \mathbf{\Phi}'(0)=0\,,\quad \mathbf{\Phi}\to 0\quad\text{as}\quad\rho\to\infty\,, \tag{A.17a}$$

$$\Delta_\rho\mathbf{N}-\frac{\nu S_0^2w^2}{b^2}\mathbf{N}=2w\mathbf{\Phi}\,,\qquad \mathbf{N}'(0)=0\,,\quad \mathbf{N}\sim\mathbf{C}\log\rho+\mathbf{B}\,,\quad\text{as}\quad\rho\to\infty\,, \tag{A.17b}$$

where $\mathbf{\Phi}\equiv(\Phi_1,\ldots,\Phi_N)$, $\mathbf{N}\equiv(N_1,\ldots,N_N)$, and where L_0 is the local operator defined in (1.4b). We then introducing the rescaling

$$\mathbf{\Phi}=\mathbf{\Phi}_0+\mathcal{O}(\nu)\,,\qquad \mathbf{N}=\nu^{-1}\mathbf{N}_0+\mathcal{O}(1)\,,\qquad \mathbf{B}=\nu^{-1}\mathbf{B}_0+\mathcal{O}(1)\,,$$

so that (A.17) becomes

$$L_0\mathbf{\Phi}_0+\frac{S_0^2w^2}{b^2}\mathbf{N}_0=\lambda\mathbf{\Phi}_0\,,\qquad \mathbf{\Phi}_0'(0)=0\,,\quad \mathbf{\Phi}_0\to 0\quad\text{as}\quad\rho\to\infty\,, \tag{A.18a}$$

(A.18b)

$$\Delta_\rho\mathbf{N}_0=\nu\left(2w\mathbf{\Phi}_0+\frac{S_0^2w^2}{b^2}\mathbf{N}_0\right)\,,\qquad \mathbf{N}_0'(0)=0\,,\quad \mathbf{N}_0\sim\nu\mathbf{C}\log\rho+\mathbf{B}_0\,,\quad\text{as}\quad\rho\to\infty\,.$$

For $\nu\ll 1$, we readily derive from (A.18) and (A.16) that $\mathbf{N}_0=\mathbf{B}_0$, and

(A.19)

$$\mathbf{C}=\int_0^\infty\left(2w\mathbf{\Phi}_0+\frac{S_0^2w^2}{b^2}\mathbf{N}_0\right)\rho\,d\rho=2\int_0^\infty\rho w\mathbf{\Phi}_0\,d\rho+\frac{S_0^2}{b}\mathbf{N}_0\,,\qquad (I+2\pi\nu\mathcal{G}_\lambda)\,\mathbf{C}=-\mathbf{N}_0\,.$$

We now eliminate $\mathbf{C}$ between the last two equations in (A.19) to determine $\mathbf{N}_0$. Upon sub-

stituting the resulting expression for $\mathbf{N}_0$ into (A.18a) we obtain a vector NLEP of the form

$$L_0\mathbf{\Phi}_0 - w^2\mathcal{H}\frac{\int_0^\infty \rho w\mathbf{\Phi}_0\,d\rho}{\int_0^\infty \rho w^2\,d\rho} = \lambda\mathbf{\Phi}_0\,, \qquad \mathcal{H} \equiv 2\left(I + \frac{b}{S_0^2}\left(I + 2\pi\nu\mathcal{G}_\lambda\right)^{-1}\right)^{-1}, \tag{A.20}$$

where $\alpha \equiv b/S_0^2 = 4\pi^2 bD_0N^2/[|\Omega|^2\mathcal{A}^2]$.

Finally, to diagonalize this vector NLEP we let $\mathbf{C}_i$ and $\kappa_{\lambda,i}$ denote the matrix spectrum of $\mathcal{G}_\lambda$, i.e.,

$$\mathcal{G}_\lambda\mathbf{C}_i = \kappa_{\lambda,i}\mathbf{C}_i\,, \qquad i = 1,\dots,N\,. \tag{A.21}$$

From the expression for $\mathcal{H}$ in (A.20) we get

$$\mathcal{H}\mathbf{C}_i = \sigma_i\mathbf{C}_i\,, \qquad i = 1,\dots,N\,; \qquad \sigma_i \equiv \frac{2(1+2\pi\nu\kappa_{\lambda,i})}{1+\alpha+2\pi\nu\kappa_{\lambda,i}}\,. \tag{A.22}$$

Upon decomposing $\mathcal{H} = \mathcal{Q}\Lambda\mathcal{Q}^T$, where Λ is the diagonal matrix of eigenvalues σ_i of $\mathcal{H}$ and $\mathcal{Q}$ is the orthogonal matrix of eigenvectors $\mathbf{C}_i$, and then introducing $\mathbf{\Psi} = \mathcal{Q}^T\mathbf{\Phi}_0$, we readily obtain the N-scalar NLEPs of the form (3.1), with multipliers as given in (3.24).

To recover the NLEP for the Schnakenberg model with the bilinear multiplier given by (1.4a) and (2.15), which is valid for $D = D_0/\nu$ and $\tau = \mathcal{O}(1)$, we first derive from (3.25) that, for $\nu \ll 1$,

$$\mathcal{G}_\lambda = \frac{D_0N}{\nu\tau\lambda|\Omega|}E + \mathcal{G}_0 + \mathcal{O}(\nu)\,, \qquad E \equiv \frac{1}{N}\mathbf{e}\mathbf{e}^T\,,$$

where $\mathbf{e} = (1,\dots,1)^T$ and $\mathcal{G}_0$ is the Neumann Green's matrix. Since $E\mathbf{e} = \mathbf{e}$ and $E\mathbf{q}_i = 0$ for $i = 2,\dots,N$, where $\mathbf{q}_i^T\mathbf{e} = 0$, the eigenvalues $\kappa_{\lambda,i}$ of $\mathcal{G}_\lambda$ are $\kappa_{\lambda,1} \sim D_0N/[\nu\tau\lambda|\Omega|]$ and $\kappa_{\lambda,i} = \mathcal{O}(1)$ for $i = 2,\dots,N$. This yields that

$$2\pi\nu\kappa_{\lambda,1} \sim \frac{\mu}{\tau\lambda}\,; \qquad 2\pi\nu\kappa_{\lambda,i} = \mathcal{O}(\nu) \quad \text{for} \quad i = 2,\dots,N\,, \tag{A.23}$$

where $\mu \equiv 2\pi ND_0/|\Omega|$. Upon substituting (A.23) into (A.22) we recover the bilinear-in-λ multipliers for the synchronous and asynchronous modes given in (2.15).

Appendix B. The Gray–Scott model. We now derive the nonlinear algebraic equation (2.20) characterizing N-spot quasi-equilibria for the GS model (1.2) when $D = D_0/\nu \gg 1$. In addition, we derive the NLEP (3.1a) with multipliers (3.34) determining the linear stability on an $\mathcal{O}(1)$ time-scale of these patterns. Since the approach is very similar to that in Appendix A we only briefly sketch the analysis here.

In the asymptotic construction of N-spot quasi-equilibria for the GS model (1.2) we obtain the same core problem (A.1) near the jth spot, while in place of (A.2), the outer solution for u now satisfies

$$\Delta u - u = -1 + \frac{2\pi\sqrt{D}}{\mathcal{A}}\sum_{i=1}^N S_i\,\delta(\mathbf{x}-\mathbf{x}_i)\,, \quad \mathbf{x}\in\Omega\,; \qquad \partial_n u = 0\,, \quad \mathbf{x}\in\partial\Omega\,, \tag{B.1a}$$

$$u \sim \frac{1}{\mathcal{A}\sqrt{D}}\left[S_j\log|\mathbf{x}-\mathbf{x}_j| + \mathcal{D}(S_j) + \frac{S_j}{\nu}\right], \quad \text{as} \quad \mathbf{x}\to\mathbf{x}_j\,, \quad j = 1,\dots,N\,, \tag{B.1b}$$

where $\nu \equiv -1/\log\varepsilon$. The solution to (B.1) is $u(\mathbf{x}) = -2\pi\left[\mathcal{A}\sqrt{D}\right]^{-1}\sum_{i=1}^{N} S_i G(\mathbf{x};\mathbf{x}_i)$, where $G(\mathbf{x};\mathbf{x}_i)$ is the reduced-wave Green's function satisfying

$$\Delta G - \frac{1}{D}G = -\delta(\mathbf{x}-\mathbf{x}_i)\,, \quad \mathbf{x}\in\Omega\,; \qquad \partial_n G = 0\,, \quad \mathbf{x}\in\partial\Omega\,, \tag{B.2a}$$

$$G(\mathbf{x};\mathbf{x}_i) = -\frac{1}{2\pi}\log|\mathbf{x}-\mathbf{x}_i| + R(\mathbf{x}_i) + o(1)\,, \quad \text{as} \quad \mathbf{x}\to\mathbf{x}_i\,. \tag{B.2b}$$

By matching the local behavior of u as $\mathbf{x}\to\mathbf{x}_j$ with the far-field behavior of the solution to each core problem, we derive in place of (A.5) that, in terms of $G_{ji}\equiv G(\mathbf{x}_j;\mathbf{x}_i)$ and $R_j \equiv R(\mathbf{x}_j)$,

$$S_j + 2\pi\nu\left(S_j R_j + \sum_{i\neq j}^{N} S_i G_{ji}\right) + \nu\mathcal{D}(S_j) = \nu\mathcal{A}\sqrt{D}\,, \quad j = 1,\dots,N\,. \tag{B.3}$$

For the parameter range $D = D_0/\nu$ with $\nu \ll 1$ we estimate $G(\mathbf{x};\mathbf{x}_i) \sim D_0/[\nu|\Omega|] + \mathcal{O}(1)$, $R(\mathbf{x}_i) \sim D_0/[\nu|\Omega|] + \mathcal{O}(1)$. Then, upon defining $\mu \equiv 2\pi N D_0/|\Omega|$, (B.3) becomes

$$S_j + \frac{\mu}{N}\sum_{i=1}^{N} S_i + \mathcal{O}(\nu) + \nu\mathcal{D}(S_j) \sim \sqrt{\nu D_0}\mathcal{A} = \sqrt{\nu\mu}\left(\mathcal{A}\sqrt{\frac{|\Omega|}{2\pi N}}\right)\,, \quad j = 1,\dots,N\,. \tag{B.4}$$

This suggests that $S_j = \mathcal{O}(\sqrt{\nu}) \ll 1$. We then look for a symmetric N-spot quasi-equilibrium for which $S_j = \sqrt{\nu}S_0$ for $j = 1,\dots,N$. We use the small-S asymptotics in (A.6) to estimate $\mathcal{D}(S_j) \sim b/[\sqrt{\nu}S_0]$. In this way, (B.4) reduces for $\nu \ll 1$ to the nonlinear algebraic equation for S_0 given in (2.20) of section 2.3.

Next, we examine the linear stability on an $\mathcal{O}(1)$ time-scale of the N-spot symmetric quasi-equilibrium solution, denoted by v_e and u_e. We linearize (1.2) about u_e, v_e to obtain the eigenvalue problem (A.8) in which $\tau\lambda$ is replaced by $(1+\tau\lambda)$. By considering only locally radially symmetric perturbations near the jth spot we derive the inner problem (A.10) provided that the consistency condition (A.11) holds. The outer problem for the perturbation in u is given by (A.13), where we replace $\tau\lambda/D$ in (A.13a) with $(1+\tau\lambda)/D$. The solution to this problem is given in (A.14), where $G_\lambda(\mathbf{x};\mathbf{x}_i)$ is the Green's function now defined by (3.3).

By asymptotically matching the inner problem for the eigenfunction to the outer problem, we obtain (A.16) in terms of the Green's matrix $\mathcal{G}_\lambda$. For the parameter range where $D = D_0/\nu \gg 1$ with $\nu \ll 1$, we can then repeat the analysis in (A.17)–(A.19) to derive the vector NLEP (A.20), where S_0 is related to the feed-rate parameter $\mathcal{A}$ through the nonlinear algebraic equation (2.20).

By diagonalizing this vector NLEP by using the eigendecomposition of $\mathcal{G}_\lambda$ as in (A.21), we readily derive (A.22) in which α is replaced by b/S_0^2. In this way, we obtain the NLEP (3.1a) with multipliers (3.34).

When $D = D_0/\nu$ and $\tau = \mathcal{O}(1)$, we can easily recover the conventional NLEP problem given by (1.4a) with the two multipliers in (2.21) for the synchronous and asynchronous modes. To do so, we use

$$\mathcal{G}_\lambda = \frac{D_0 N}{\nu(1+\tau\lambda)|\Omega|}E + \mathcal{G}_0 + \mathcal{O}(\nu)\,, \qquad E \equiv \frac{1}{N}\mathbf{e}\mathbf{e}^T\,,$$

for $\nu \ll 1$ to estimate the eigenvalues $\kappa_{\lambda,i}$ of $\mathcal{G}_\lambda$ as $\kappa_{\lambda,1} \sim D_0 N/\left[\nu(1+\tau\lambda)|\Omega|\right]$ and $\kappa_{\lambda,i} = \mathcal{O}(1)$ for $i = 2, \ldots, N$. By substituting these expressions into (3.34) we readily obtain (2.21).

Appendix C. The Gierer–Meinhardt model. We now derive the NLEP (3.1a) with multipliers (3.1b) determining the linear stability on an $\mathcal{O}(1)$ time-scale of N-spot quasi-equilibria for the GM model (1.1), valid for arbitrary τ. Our approach is different than in Appendix A in that we follow [27] and develop only a leading-order theory in ν for the regime $D = D_0/\nu$. We set $D = D_0/\nu$ with $\nu = -1/\log\varepsilon$ and write (1.1) as

$$v_t = \varepsilon^2 \Delta v - v + v^2/u\,, \qquad \tau u_t = \frac{D_0}{\nu}\Delta u - u + \varepsilon^{-2} v^2\,, \qquad \mathbf{x} \in \Omega\,. \tag{C.1}$$

To leading order in ν, we first construct an N-spot quasi-equilibrium solution for (C.1). In the inner region near $\mathbf{x} = \mathbf{x}_j$ we define $\mathbf{y} = \varepsilon^{-1}(\mathbf{x} - \mathbf{x}_j)$ with $\rho = |\mathbf{y}|$ and look for a locally radially symmetric solution in the form $v \sim \mathcal{V}_j(\rho)$ and $u \sim \mathcal{U}_j(\rho)$. From the steady-state equations of (C.1), we get on $0 < \rho < \infty$ that $\mathcal{V}_j$ and $\mathcal{U}_j$ satisfy

$$\Delta_\rho \mathcal{V}_j - \mathcal{V}_j + \mathcal{V}_j^2/\mathcal{U}_j = 0\,, \quad \mathcal{V}_j \to 0 \quad \text{as} \quad \rho \to \infty\,; \qquad \Delta_\rho \mathcal{U}_j = \frac{\nu}{D_0}\mathcal{V}_j^2\,, \tag{C.2}$$

where $\Delta_\rho \equiv \partial_{\rho\rho} + \rho^{-1}\partial_\rho$. For $\nu \ll 1$, we expand $\mathcal{U}_j = \mathcal{U}_{j0} + \nu\mathcal{U}_{j1} + \cdots$, to obtain that $\mathcal{U}_{j0}$ is a constant. Then, from the first equation in (C.2) we get $\mathcal{V}_j \sim \mathcal{U}_{j0} w$, where $w(\rho)$ is the ground-state solution (1.4c). From the second equation in (C.2) we conclude that $\Delta_\rho \mathcal{U}_{J1} = -\mathcal{U}_{j0}^2 w^2/D_0$, which yields the far-field behavior

$$\mathcal{U}_{j1} \sim -\frac{\mathcal{U}_{j0}^2}{D_0} b \log\rho + \mathcal{O}(1)\,, \quad \text{as} \quad \rho \to \infty\,; \qquad b \equiv \int_0^\infty \rho w^2\, d\rho\,. \tag{C.3}$$

By matching the far-field of each inner solution $\mathcal{U}_J$ to an outer solution, we get the outer problem for u

$$\frac{D_0}{\nu}\Delta u - u = -2\pi b \sum_{i=1}^N \mathcal{U}_{i0}^2 \delta(\mathbf{x} - \mathbf{x}_i)\,, \quad \mathbf{x} \in \Omega\,; \qquad \partial_n u = 0\,, \quad \mathbf{x} \in \partial\Omega\,, \tag{C.4a}$$

$$u \sim \mathcal{U}_{j0} - \frac{\mathcal{U}_{j0}^2 b}{D_0} - \nu\left(\frac{\mathcal{U}_{j0}^2 b}{D_0}\log|\mathbf{x} - \mathbf{x}_j| + \mathcal{O}(1)\right)\,, \quad \text{as} \quad \mathbf{x} \to \mathbf{x}_j\,, \quad j = 1, \ldots, N\,, \tag{C.4b}$$

where $\nu \equiv -1/\log\varepsilon$. Upon expanding $u = u_0 + \nu u_1 + \cdots$, we obtain that u_0 is a constant and that $u_0 = \mathcal{U}_{j0} - \mathcal{U}_{j0}^2 b/D_0$ for $j = 1, \ldots, N$. We obtain that u_1 satisfies

$$D_0 \Delta u_1 = u_0 - 2\pi b \sum_{i=1}^N \mathcal{U}_{i0}^2 \delta(\mathbf{x} - \mathbf{x}_i)\,, \quad \mathbf{x} \in \Omega\,; \qquad \partial_n u_1 = 0\,, \quad \mathbf{x} \in \partial\Omega\,, \tag{C.5a}$$

$$u_1 \sim -\left(\frac{\mathcal{U}_{j0}^2 b}{D_0}\log|\mathbf{x} - \mathbf{x}_j| + \mathcal{O}(1)\right)\,, \quad \text{as} \quad \mathbf{x} \to \mathbf{x}_j\,, \quad j = 1, \ldots, N\,. \tag{C.5b}$$

From the divergence theorem, we require that $u_0|\Omega| = 2\pi b\sum_{i=1}^N \mathcal{U}_{i0}^2$. In this way, we obtain that $\mathcal{U}_{j0}$ for $j = 1,\dots,N$ satisfies the nonlinear algebraic system

$$\frac{2\pi b}{|\Omega|}\sum_{i=1}^N \mathcal{U}_{i0}^2 = \mathcal{U}_{j0} - \frac{b\mathcal{U}_{j0}^2}{D_0}\,, \quad j = 1,\dots,N\,. \tag{C.6}$$

For a symmetric N-spot quasi-equilibrium solution we set $\mathcal{U}_{j0} = \mathcal{U}_0$ for $j = 1,\dots,N$. From (C.6) we obtain that

$$\mathcal{U}_0 = \frac{D_0}{b(\mu+1)}\,, \qquad \text{where} \qquad \mu \equiv \frac{2\pi N D_0}{|\Omega|}\,, \qquad b \equiv \int_0^\infty \rho w^2\,d\rho\,. \tag{C.7}$$

Then, from (C.5), $u_1 = 2\pi b\mathcal{U}_0^2 D_0^{-1}\left[\sum_{i=1}^N G_0(\mathbf{x};\mathbf{x}_i) + \bar{u}_1\right]$, where G_0 is the Neumann Green's function of (A.4) and $\bar{u}_1$ is a constant.

Next, we examine the linear stability of N-spot symmetric quasi-equilibria, denoted by v_e and u_e. Upon introducing $u = u_e + e^{\lambda t}\eta$ and $v = v_e + e^{\lambda t}\phi$ into (C.1) and linearizing, we obtain the eigenvalue problem

$$\varepsilon^2\Delta\phi - \phi + \frac{2v_e}{u_e}\phi - \frac{v_e^2}{u_e^2}\eta = \lambda\phi\,, \qquad \frac{D_0}{\nu}\Delta\eta - (1+\tau\lambda)\eta = -2\varepsilon^{-2}v_e\phi\,, \qquad \mathbf{x}\in\Omega\,, \tag{C.8}$$

with $\partial_n\phi = \partial_n\eta = 0$ on $\partial\Omega$. In the inner region near the jth spot, where $v_e \sim \mathcal{U}_0 w(\rho)$ and $u_e \sim \mathcal{U}_0$ with $\rho = \varepsilon^{-1}|\mathbf{x}-\mathbf{x}_j|$, we look for a leading-order locally radially symmetric solution of the form $\phi \sim \Phi_j(\rho)$ and $\eta \sim N_j(\rho)$. From (C.8) we get in terms of the local operator L_0 of (1.4b) that on $0 < \rho < \infty$,

$$L_0\Phi_j - w^2 N_j = \lambda\Phi_j\,, \qquad \Delta_\rho N_j = -\frac{2\mathcal{U}_0\nu}{D_0}w\Phi_j\,, \tag{C.9}$$

provided that τ satisfies $\varepsilon^2\tau\lambda\nu/D_0 \ll 1$ (see (A.11). We then expand $\Phi_j = \Phi_{j0} + \cdots$ and $N_j = N_{j0} + \nu N_{j1} + \cdots$ to obtain that N_{j0} is a constant and that $\Delta_\rho N_{j1} = -2\mathcal{U}_0 w\Phi_j/D_0$. This yields that N_j has the far-field behavior

$$N_j \sim N_{j0} - \nu\left[\frac{2\mathcal{U}_0}{D_0}\left(\int_0^\infty \rho w\Phi_{0j}\,d\rho\right)\log\rho + \mathcal{O}(1)\right]\,, \quad \text{as} \quad \rho\to\infty\,. \tag{C.10}$$

Upon matching the far-field behavior of the inner solution N_j to an outer solution, we obtain that the outer problem for η is

(C.11a)

$$\Delta\eta - \frac{\nu}{D_0}(1+\tau\lambda)\,\eta = -\frac{4\pi\mathcal{U}_0\nu}{D_0}\sum_{i=1}^N\left(\int_0^\infty \rho w\Phi_{0i}\,d\rho\right)\delta(\mathbf{x}-\mathbf{x}_i)\,, \quad \mathbf{x}\in\Omega\,; \quad \partial_n\eta = 0\,, \quad \mathbf{x}\in\partial\Omega\,,$$

(C.11b)

$$\eta \sim N_{j0} - \frac{2\mathcal{U}_0}{D_0}\left(\int_0^\infty \rho w\Phi_{0j}\,d\rho\right) - \nu\left[\frac{2\mathcal{U}_0}{D_0}\left(\int_0^\infty \rho w\Phi_{0j}\,d\rho\right)\log|\mathbf{x}-\mathbf{x}_j| + \mathcal{O}(1)\right]\,, \quad \text{as} \quad \mathbf{x}\to\mathbf{x}_j\,,$$

for $j = 1, \ldots, N$. The solution to (C.11a) is

$$\eta = \frac{4\pi \mathcal{U}_0 \nu}{D_0} \sum_{i=1}^{N} G_\lambda(\mathbf{x}; \mathbf{x}_i) \left(\int_0^\infty \rho w \Phi_{0i} \, d\rho \right) , \tag{C.12}$$

where $\mathcal{G}_\lambda$ is the reduced-wave Green's function satisfying (3.3). By enforcing that the non-singular term of the local behavior of η as $\mathbf{x} \to \mathbf{x}_j$ agrees with that in (C.11b), we determine $\mathbf{N}_0 \equiv (N_1, \ldots, N_N)^T$ as

$$\mathbf{N}_0 = \frac{2\mathcal{U}_0}{D_0} \left[I + 2\pi\nu \mathcal{G}_\lambda \right] \left(\int_0^\infty \rho w \boldsymbol{\Phi}_0 \, , d\rho \right) , \tag{C.13}$$

where $\mathcal{G}_\lambda$ is the Green's matrix of (3.2). Upon using (C.7) for $\mathcal{U}_0/D_0$, and substituting (C.13) into the first equation of (C.9), we obtain the vector NLEP

$$L_0 \boldsymbol{\Phi}_0 - w^2 \mathcal{H} \frac{\int_0^\infty \rho w \boldsymbol{\Phi}_0 \, d\rho}{\int_0^\infty \rho w^2 \, d\rho} = \lambda \boldsymbol{\Phi}_0 \, , \qquad \text{where} \qquad \mathcal{H} \equiv \frac{2}{\mu + 1} \left(I + 2\pi\nu \mathcal{G}_\lambda \right) . \tag{C.14}$$

By diagonalizing this vector NLEP, as in (A.22), we obtain the NLEP (3.1a) with the N multipliers in (3.1b).

REFERENCES

[1] M. Abramowitz and I. Stegun, *Handbook of Mathematical Functions*, 9th ed., Dover, New York.

[2] W. Chen and M. J. Ward, *Oscillatory instabilities and dynamics of multi-spike patterns for the one-dimensional Gray–Scott model*, European J. Appl. Math., 20 (2009), pp. 187–214.

[3] W. Chen and M. J. Ward, *The stability and dynamics of localized spot patterns in the two-dimensional Gray–Scott model*, SIAM J. Appl. Dyn. Syst., 10 (2011), pp. 582–666.

[4] A. Doelman and F. Veerman, *An explicit theory of pulses in two component, singularly perturbed, reaction-diffusion equations*, J. Dynam. Differential Equations, 27 (2015), pp. 555–595.

[5] A. Doelman, R. A. Gardner, and T. Kaper, *A Stability Index Analysis of 1-D Patterns of the Gray Scott Model*, Mem. Amer. Math. Soc. 155, AMS. Providence, RI, 2002.

[6] A. Doelman, R. A. Gardner, and T. Kaper, *Large stable pulse solutions in reaction-diffusion equations*, Indiana Univ. Math. J., 50 (2001), pp. 443–507.

[7] FlexPDE6, *PDE Solutions*, http://www.pdesolutions.com.

[8] J. Gou and M. J. Ward, *Asymptotic analysis of a 2-D model of dynamically active compartments coupled by bulk diffusion*, J. Nonlinear Sci., 16 (2016), pp. 979–1029.

[9] D. Iron, J. Rumsey, M. J. Ward, and J. Wei, *Logarithmic expansions and the stability of periodic patterns of localized spots for reaction-diffusion systems in* $\mathbb{R}^2$, J. Nonlinear Sci., 24 (2014), pp. 857–912.

[10] T. Kolokolnikov and M. J. Ward, *Reduced wave Green's functions and their effect on the dynamics of a spike for the Gierer–Meinhardt model*, European J. Appl. Math., 14 (2003), pp. 513–545.

[11] T. Kolokolnikov, M. J. Ward, and J. Wei, *Spot self-replication and dynamics for the Schnakenberg model in a two-dimensional domain*, J. Nonlinear Sci., 19 (2009), pp. 1–56.

[12] T. Kolokolnikov, M. J. Ward, J. Wei, *The existence and stability of spike equilibria in the one-dimensional Gray–Scott model: The low feed rate regime*, Stud. Appl. Math., 115 (2005), pp. 21–71.

[13] M. C. Kropinski and B. D. Quaife, *Fast integral equation methods for the modified Helmholtz equation*, J. Comput. Phys., 230 (2011), pp. 425–434.

[14] C. S. Lin, W. M. Ni, and I. Takagi, *Large amplitude stationary solutions to a chemotaxis system*, J. Differential Equations, 72 (1988), pp. 1–27.

[15] Y. Nishiura, *Far-from Equilibrium Dynamics, Translations of Mathematical Monographs*, Vol. 209, AMS, Providence, RI, 2002.
[16] J. E. Pearson, *Complex patterns in a simple system*, Science, 216 (1993), pp. 189–192.
[17] I. Rozada, S. Ruuth, and M. J. Ward, *The stability of localized spot patterns for the Brusselator on the sphere*, SIAM J. Appl. Dyn. Syst., 13 (2014), pp. 564–627.
[18] P. H. Trinh and M. J. Ward, *The dynamics of localized spot patterns for reaction-diffusion systems on the sphere*, Nonlinearity, 29 (2016), pp. 766–806.
[19] J. C. Tzou and M. J. Ward, *Effects of open systems on the existence, dynamics, and stability of spot patterns in the* 2*D Brusselator model*, Phys. D, to appear.
[20] J. Tzou, Y. Nec, and M. J. Ward, *The stability of localized spikes for the* 1*-D Brusselator reaction diffusion model*, European J. Appl. Math., 24 (2013), pp. 515–564.
[21] V. K. Vanag and I. R. Epstein, *Localized patterns in reaction-diffusion systems*, Chaos, 17 (2007), 037110.
[22] F. Veerman, *Breathing pulses in singularly perturbed reaction-diffusion systems*, Nonlinearity, 28 (2015), pp. 2211–2246.
[23] S. Xie and T. Kolokolnikov, *Moving and jumping spot in a two dimensional reaction-diffusion model*, Nonlinearity, to appear.
[24] M. J. Ward and J. Wei, *Hopf bifurcation of spike solutions for the shadow Gierer–Meinhardt model*, European J. Appl. Math., 14 (2003), pp. 677–711.
[25] M. J. Ward and J. Wei, *Hopf bifurcation and oscillatory instabilities of spike solutions for the one-dimensional Gierer–Meinhardt model*, J. Nonlinear Sci., 13 (2003), pp. 209–264.
[26] J. Wei, *On single interior spike solutions of the Gierer–Meinhardt system: Uniqueness and spectrum estimates*, European J. Appl. Math., 10 (1999), pp. 353–378.
[27] J. Wei and M. Winter, *Spikes for the two-dimensional Gierer–Meinhardt system: The weak coupling case*, J. Nonlinear Sci., 11 (2001), pp. 415–458.
[28] J. Wei, *Pattern formations in two-dimensional Gray–Scott model: Existence of single-spot solutions and their stability*, Phys. D, 148 (2001), pp. 20–48.
[29] J. Wei and M. Winter, *Asymmetric spotty patterns for the Gray–Scott model in* $\mathbb{R}^2$, Stud. Appl. Math., 110 (2003), pp. 63–102.
[30] J. Wei and M. Winter, *Existence and stability of multiple spot solutions for the Gray–Scott model in* $\mathbb{R}^2$, Phys. D, 176 (2003), pp. 147–180.
[31] J. Wei and M. Winter, *Stationary multiple spots for reaction-diffusion systems*, J. Math. Biol., 57 (2008), pp. 53–89.
[32] J. Wei, *Existence and stability of spikes for the Gierer–Meinhardt system*, in Handbook of Differential Equations, Stationary Partial Differential Equations, Vol. 5: M. Chipot, ed., Elsevier, New York, 2008, pp. 489–581.
[33] J. Wei and M. Winter, *Mathematical Aspects of Pattern Formation in Biological Systems*, Appl. Math. Sci. Ser. 189, Springer, New York, 2014.